UAB

Master's Thesis

Master in Telecommunication Engineering

Application of Artificial Transmission Lines Based on Inductive Loading to Filter Design

Claudia Nicolini Teixidor

Supervisors: Ferran Martín Antolín
Paris Vélez Rasero

Department of Electronic Engineering

Escola d'Enginyeria
Universitat Autònoma de Barcelona (UAB)

July 2019

Els sotasignants, *Ferran Martín Antolín* i *Paris Vélez Rasero*, Professors de l'Escola d'Enginyeria de la Universitat Autònoma de Barcelona (UAB),

CERTIFIQUEN:

Que el projecte presentat en aquesta memòria de Treball Final de Màster ha estat realitzat sota la seva direcció per l'alumne *Claudia Nicolini Teixidor*.

I, perquè consti a tots els efectes, signen el present certificat.

Bellaterra, *3 de juliol de 2019*.

Signatura: *Ferran Martín Antolín* *Paris Vélez Rasero*

Resum:

Un dels problemes més importants a l'hora de dissenyar filtres de microones, sovint, és poder complir amb tots els paràmetres establerts i seguir sent físicament implementables. És per això, que s'ha decidit aplicar la teoria de les línies de transmissió artificials a un filtre de rebuig de banda basat en ressonadors $\lambda/4$.

Les línies de transmissió artificials es basen en introduir elements reactius, com inductàncies i capacitàncies a les línies convencionals seguint una distribució periòdica i reduint així la seva velocitat de propagació, d'aquesta manera, s'aconsegueixen eliminar espúries i reduir la mida física del dispositiu de manera controlada. Aquesta última situació és ideal quan en una determinada aplicació, es requereix reduir la mida per a que el dispositiu pugui ser implementat físicament en un substrat en concret obtenint el mateix comportament a la freqüència d'operació.

Resumen:

Uno de los problemas más importantes a la hora de diseñar filtros de microondas, es poder cumplir con todos los parámetros establecidos y seguir siendo físicamente implementables. Por ello, se ha decidido aplicar la teoría de las líneas de transmisión artificiales a un filtro supresor de banda basado en resonadores $\lambda/4$.

Las líneas de transmisión artificiales se basan en introducir elementos reactivos, como inductancias y capacitancias a las líneas convencionales siguiendo una distribución periódica y, por lo tanto, reduciendo su velocidad de propagación, de esta forma, se consigue eliminar espurios y reducir el tamaño del dispositivo de manera controlada. Esta última situación es ideal cuando en una determinada aplicación se requiere reducir el tamaño para que el dispositivo pueda ser implementado físicamente en un substrato concreto obteniendo el mismo comportamiento en la frecuencia de operación.

Summary:

One of the most important problems when designing microwave filters, is being able to accomplish all the stablished parameters and still being physically implementable. For that reason, it has been decided to apply the theory of artificial transmission lines into a stopband filter based on $\lambda/4$ resonators.

The artificial transmission lines are based on introducing reactive elements, such as inductances or capacitances, to the conventional lines following a periodic distribution and, therefore, reducing the propagation velocity of the line. This way, it is possible to cancel spurious frequencies and reduce the size of the device in a controlled manner. This last situation is ideal when in a determined application it is required to reduce the size of the device in order to be implemented physically on the specific substrate obtaining the same behavior at the frequency of operation.

CONTENTS

LIST OF FIGURES

1. INTRODUCTION

The purpose of this chapter is to clarify the reasons of developing this thesis, how it has been developed and the main causes that have generated the motivation of its realization. Bellow will be explained the objectives that this thesis wants to achieve and eventually, a state of the art in order to highlight some of the existing studies that have been provided using the techniques that are used in this thesis.

1.1 Thesis Motivation

Ordinary transmission lines have some limitations from the fact that they have a limited number of free parameters for design purposes. For that reason, it can sometimes be difficult or even impossible to implement an ordinary line with specific desing parameters.

Artificial transmission lines are very useful in the RF and Microwave fields as by truncating the uniformity and loading the line with reactive elements there appear more degrees of freedom than in the ordinary transmission lines. Not only that, but also there appear many options to reduce the size of the device, improve its performance or even achieve new functionalities.

This technology is applicable to this thesis as some microwave filters have problems at the time of defining its parameters and the implementation of the filter. Sometimes the filter is not implementable with the exact specifications wanted by the user, for instance, a specific bandwidth can generate too high values of impedances that produce the impossible physical implementation of the filter as, depending on the substrate, the lines might have very narrow widths.

This idea is applicable to this thesis as one of the characteristics of a kind of stopband filters is that the impedances of the stubs in which such filters are based are very high in order to be implementable. By applying this technology to these filters, the impedance value of the stubs is reduced accomplishing its possible implementation.

1.2 Thesis Definition

The main idea of this thesis consists on applying the theory of artificial transmission lines on a stopband filter operating at 1GHz that is characterized of having very high impedances stubs, which carries out to a very small width of the lines and, as a consequence, it can be unimplementable. Introducing this technology, the impedances will be reduced and consequently, the filter will be implementable. The relevant characteristics of this filter will be introduced in order to explain how this theory can be applied on it.

The artificial transmission lines rely on the idea of introducing perturbations, as reactive elements (such as capacitors, inductors, etc.) in a conventional transmission line. By introducing a periodic distribution of these elements, it can be achieved a smaller phase velocity than the conventional one, and so, a smaller wavelength, while operating at the same frequency. This is due to the presence of the reactive elements, because there are more free parameters in the line and hence, further controllability of the main line parameters, which are the characteristic impedance and the phase constant. [1]

The filter that will be designed is based on $\lambda/4$ resonators and it consists of a main host line with section of 90º and a characteristic impedance of $Z_0 = 50\Omega$ with shunt stubs ended with an open or short circuit, depending on the case, all of them having an electrical length of 90º.

These filters are based on the fact that a line section at $\lambda/4$ ended with open circuit or short circuit behaves as series or parallel LC circuit. For the case of ending the line with an open circuit, the filter will be a stopband filter, and, on the contrary, for the case of ending it with short circuit, it will be a bandpass filter.

On this thesis, the stopband filter has been chosen in order to realize the study, for that case, the stubs are ended with an open circuit as shown below:

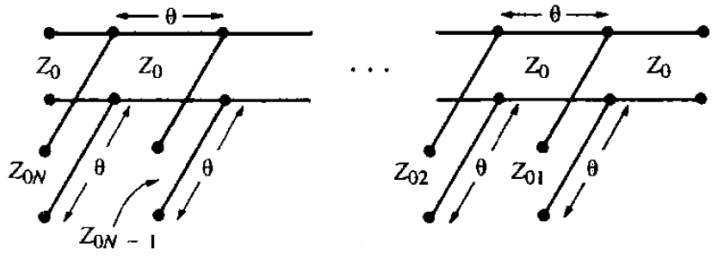

Figure 1.1: Structure of a stopband filter based on $\lambda/4$ resonators

A section of the line has the same behavior as series LC resonator near the operating frequency in which the line has a length of $\lambda/4$, giving the following relation:

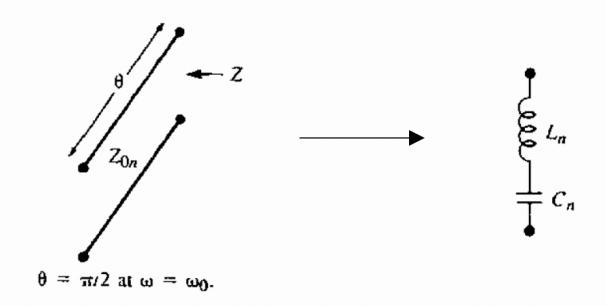

Figure 1.2: Behavior of a section of the line

The parameters that have been decided to apply in order to realize this study are the following:

- Relative Bandwidth: 30%
- Filter Response: Chebyshev 0.5dB ripple
- Order of the filer: $N = 5$
- Operating (central) frequency: 1GHz

As the order of the filter has been decided to be $N = 5$, the filter will be composed of five cascaded stubs and a host line, in which the electrical length between each stub will be 90º.

Later on, it will be exposed that this filter with these characteristics is impossible to be implemented as the impedances of the stubs, Z_{on}, are very high and consequently, the lines are very narrow to be implemented on the desired substrate.

The theory of artificial transmission lines can be defined as the introduction of reactive elements loading a conventional transmission line following a periodic distribution and having a small phase velocity compared to the ordinary transmission line.

The main idea, is that by applying the artificial transmission lines theory to this filter, not only the size of the device will be reduced, but the stub impedances will be lower by introducing an inductive load to the lines, and so, it will be possible to implement the filter.

1.3 Thesis Objectives

Once the thesis definition has been exposed, in order to focus the project goals, the objectives of this thesis have been defined.

The main objective is to reduce the filter's size compared to the ordinary one without altering the behavior at the operating frequency in terms of bandwidth.

Another objective is to not increase the design complexity of the filter, as this improvement will be done by introducing reactive elements to the stubs of the filter.

The cost of the implementation should not be increased. By applying artificial transmission lines, no additional materials or techniques should be necessary, and no different substrates should be taken in mind.

In order to accomplish these objectives, they have been kept in mind during the development of the thesis.

1.4 State of the Art

Several research groups have taken in to account the potential properties of the artificial transmission lines. In a specific RF device, the size reduction and the elimination of spurious frequencies are usually desired. Moreover, as stated previously, the application of this technique does not usually imply an increase in the cost of the device.

In order to see what this technique is capable of, let us expose some real implementations of these research groups in order to see several designs where this technique is applied.

For instance, let us suppose a capacitively loaded coupled-line bandpass filter [2] as shown in the figure 1.3. This study compares the conventional filter and the same filter where patch capacitors have been loaded periodically.

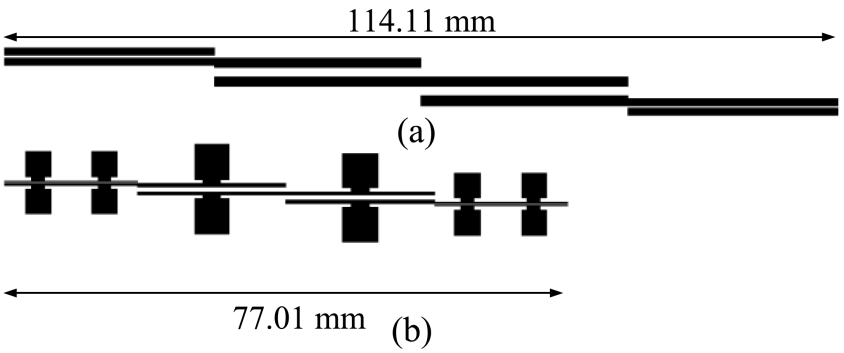

Figure 1.3: Layouts of the designed coupled-line bandpass filters. (a) Convectional. (b) Capacitively loaded [2]

By comparing both topologies, it can be appreciated that there is a miniaturization factor. This miniaturization feature was expected, since this is a known characteristic of this technique. At this point, the frequency response of these filters is represented in figure 1.4.

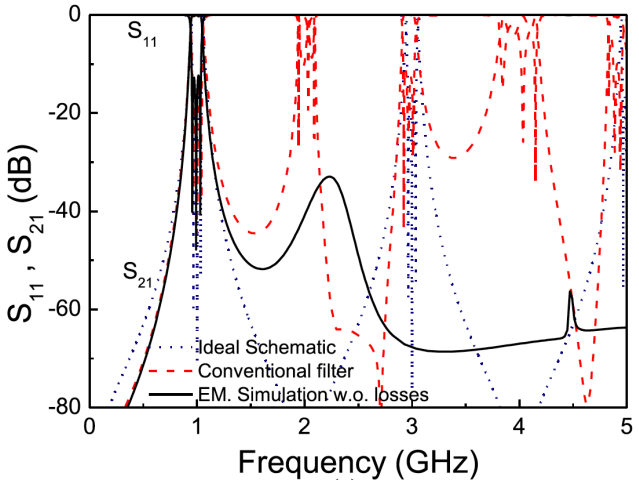

Figure 1.4: Frequency responses of both topologies of the filter [2]

In this figure, the responses of both filters are shown, where the presence of spurious bands, at $2f_0$ and at higher frequencies can be appreciated. The conventional filter topology allows harmonic frequency bands, whereas the capacitively-loaded filter is able to cancel them without affecting at the frequency of operation. In figure 1.5, the same response is zoomed-in in order to appreciate it at the frequency of interest.

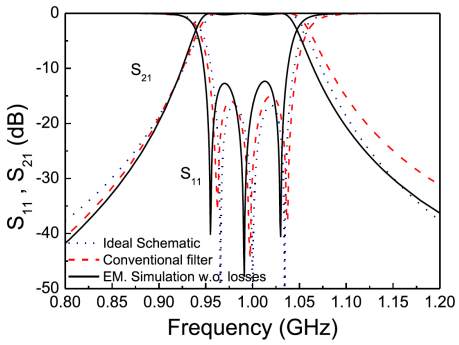

Figure 1.5: Zoomed-in view of the passband [2]

Furthermore, in figure 1.6 there is another example that applies the same technique, this study consists on the design and implementation of a compact power splitter with harmonic suppression but in this case, by means of inductively and capacitively loaded transmission lines [3].

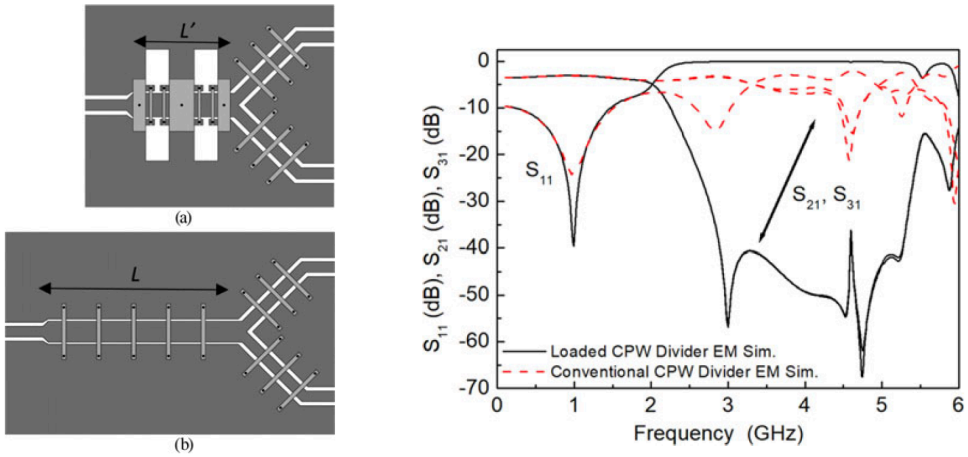

Figure 1.6: Layouts of the slow-wave (a) and ordinary (b) power splitters and frequency response comparison [3]

As it can be seen in the previous figure, there has been a size reduction due to implementing the splitter by means of artificial transmission lines, where in figure 1.6 (a) it can be appreciated that the artificial line consists of two unit cells that include both, inductive slots and capacitive strips. According to the response, it is shown how the loaded splitter maintains the same behavior at the operating frequency, whereas the first two harmonic bands have been attenuated.

In addition, there is another research study that implements the slow-wave structures to a compact coplanar waveguide (CPW) power splitter in order to efficiently shorten the length of the inverters and thereby, providing a substantial size reduction and harmonic suppression to the power splitter [4].

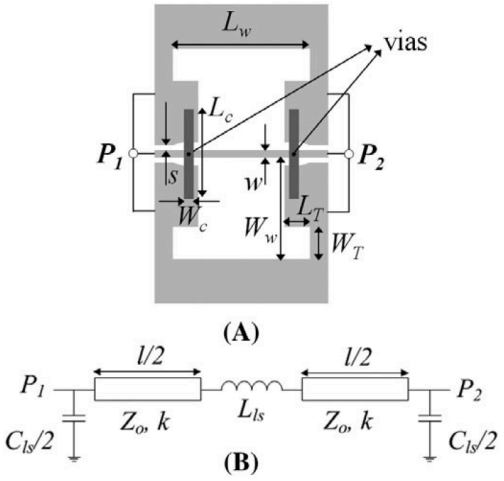

Figure 1.7: Topology of the unit cell (A) and circuit schematic (B) of the slow-wave CPW transmission line [4]

In this case, the CPW is loaded with a series inductance, L_{ls}, implemented by means of a pair of symmetric slots etched in the ground plane and with a pair of shunt capacitances, $C_{ls}/2$, by means of two patches etched in the back substrate side and connected to the central strip through a vias.

Figure 1.8 represents the layout of the power splitter, which has been implemented with two unit cells ($N = 2$).

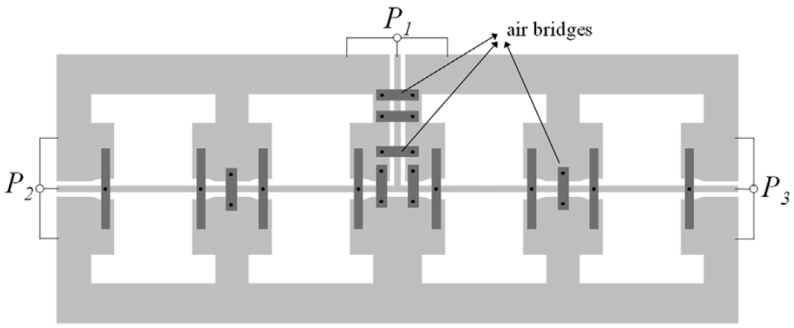

Figure 1.8: Layout of the designed power splitter [4]

The splitter dimensions are mainly determined by the length of the synthesized slow-wave impedance inverter. The ratio between the length of the designed inverter and the ordinary one is 0.505, which is slightly superior than the theoretical value given by the swr, which was established to 0.5, however, the achieved size reduction is very close to the theoretical value.

Finally, the response of the splitter is shown in figure 1.9, where it can be seen that the response of the slow-wave power splitter is roughly the same than the one of the ordinary splitter in the region of interest (vicinity of f_0).

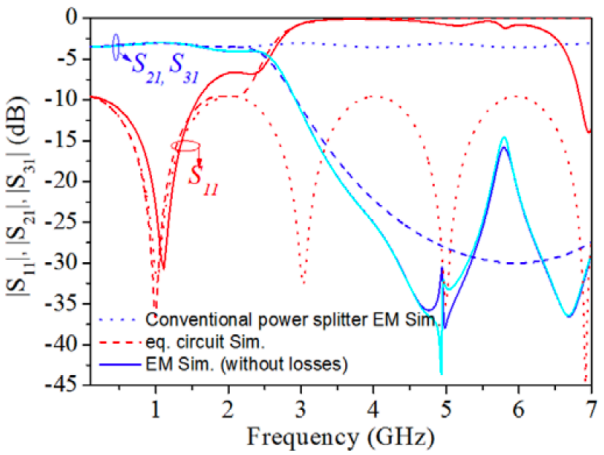

Figure 1.9: Response of the splitter, including matching (S_{11}) and power splitting (S_{21} and S_{31}) [4]

2. ARTIFICIAL TRANSMISSION LINES

In this chapter, the theory of artificial transmission lines will be exposed in order to provide a clear understanding of the development of this thesis. The purpose of this chapter is to briefly present the Floquet analysis of one-dimensional periodic structures and the transfer matrix method, applied to the unit cell for obtaining the dispersion curves of the fundamental harmonics. Finally, the Bloch impedance concept will be exposed.

2.1 Floquet's Theorem

In order to explain the Floquet's Theorem, it must be considered a one-dimensional infinite periodic structure, such as a periodically perturbated infinite transmission line with a period l and the propagation axis z.

The Floquet's Theorem states that the fields propagating along the line can be expressed as Bloch waves according to:

$$\Psi(z) = e^{\gamma z} \cdot P(z) \tag{2.1}$$

where $P(z)$ corresponds to a periodic function with period l and γ is the propagation constant,

$$\gamma = \alpha + j\beta \tag{2.2}$$

The following condition can be also established, as $P(z)$ is a periodic function,

$$P(z) = P(z + l) \tag{2.3}$$

According to these equations, the field behavior can be expressed in terms of a fundamental wave, where $P(z)$ is the standing wave that is repeated to each unit cell and represents the local variations due to the periodicity.

Hence, the fields propagating along the line satisfy that,

$$\Psi(z + l) = e^{-\gamma(z+l)} \cdot P(z + l) = e^{-\gamma l} \cdot \Psi(z) \tag{2.4}$$

Which stands that the fields of a Bloch wave, are repeated at each unit cell having a propagation factor of $e^{-\gamma l}$.

As $P(z)$ is a periodic function, it can be expanded in a Fourier series as

$$P(z) = \sum_{n=-\infty}^{n=+\infty} P_n e^{-j\frac{2\pi n}{l}z} \tag{2.5}$$

And the fields can now be expressed as

$$\Psi(z) = \sum_{n=-\infty}^{n=+\infty} P_n e^{-j\left(\beta+\frac{2\pi n}{l}\right)z} \cdot e^{-\alpha z} \tag{2.6}$$

The field components are called space harmonics, and β corresponds to the phase constants of these space harmonics, given by

$$\beta_n = \beta + \frac{2\pi n}{l} \qquad\qquad n = 0, \pm 1, \pm 2, \ldots \tag{2.7}$$

According to this, the phase of the fundamental harmonic where $n = 0$, $\beta_0 = \beta$. This would correspond to the case where the wave is propagating through an ordinary transmission line, only the fundamental propagating mode is going to appear at the structure. When periodic perturbations are added to the transmission line, all the n modes are going to appear contributing to the whole field distributed in the structure.

The group velocity is the same for all the harmonics, as the phase constants of the space harmonics differ by a constant, and it is determined by the following expression,

$$v_{gn} = \frac{d\omega}{d\beta} \tag{2.8}$$

And the phase velocities are given by

$$v_{pn} = \frac{\omega}{\beta + \frac{2\pi n}{l}} \tag{2.9}$$

As the phase velocities of the space harmonics are similar and the group velocities are opposite it is possible to obtain the pass/stop band characteristics. The coupling between these modes propagating through the structure contributes to the fact that some

frequencies are not going to be allowed to be propagated through the structure. This can be seen in figure 2.1, where the ω vs βl dispersion diagram for a periodically perturbed transmission line is represented, and for the fundamental harmonic, as the group and phase velocity are the same, it can be represented as a straight line, but for the case of the space harmonics, this can be represented as parallel lines to the fundamental one (the difference between the fundamental harmonic and the rest of the space harmonics, as stated in (2.7) is a shift of $2\pi n/l$).

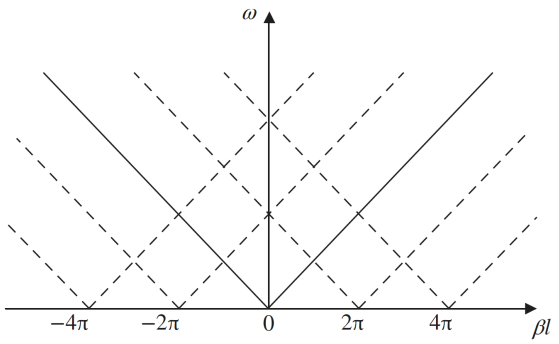

Figure 2.1: $\beta - \omega$ diagram of the space harmonics

According to figure 2.1, the dispersion lines of the different space harmonics are matched at the frequencies which satisfy $\beta l = n\pi$ (with $n = \pm 1, \pm 2, ...$). At these points, the phase velocities of both harmonics are equal, but the group velocities are opposite (since the slope of each one is opposite), and thus, the contribution of each space harmonic gets cancelled by the contribution of the other one. This fact generates a band gap at these frequencies, that will always follow the condition of $\beta l = n\pi$, and for the specific case of $n = \pm 1$, then $l = \lambda/2$.

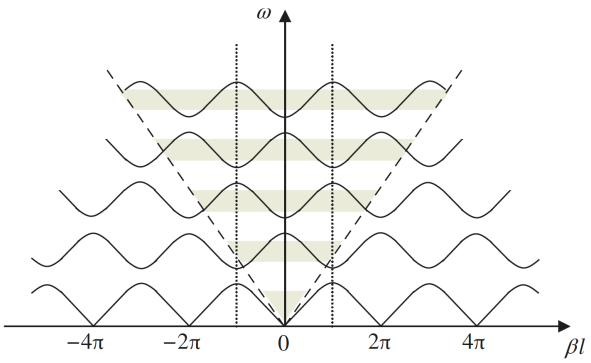

Figure 2.2: Dispersion diagram of a one-dimensional periodic structure with space harmonics with stop bands

If this condition is inserted in the frequency expression of $f = v_p/\lambda$, taking into account that $\beta = 2\pi/\lambda$, the first frequency that satisfies the stop band condition is

$$f = \frac{v_p}{2l} \tag{2.10}$$

where v_p corresponds to the phase velocity of the ordinary transmission line.

This expression is known as the Bragg condition and stated that the first stop band caused by the effects of periodicity appears at the frequency satisfying that the period is half the wavelength of the unperturbed line, λ.

2.2 ABCD Transfer Matrix

In order to obtain the dispersion characteristics of the fundamental space harmonic, or equivalently the Bloch wave, it is necessary to explain the ABCD Transfer Matrix as its application model, which is capable of describing in a proper manner the behavior of the Bloch waves, or dispersion of fundamental harmonics. The concept of the ABCD transfer matrix, by definition, allows to obtain the ABCD matrix of a two ports network by multiplying the ABCD matrix of the cascaded elements that compose the network [5] (in this case, a periodic structure with a unit cell).

Let us consider the following periodic structure:

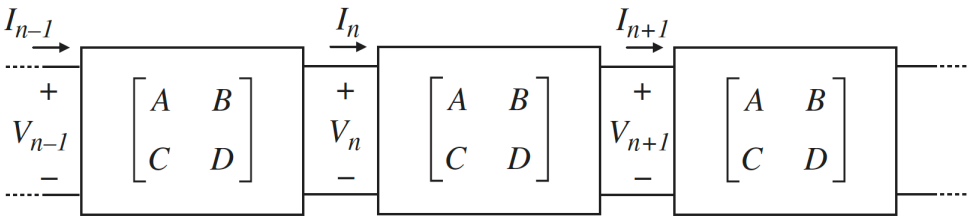

Figure 2.3: ABCD transfer matrix representation of a periodic structure with unit cell

The voltages and currents of both sides of the network, or unit cell, are related by the ABCD matrix according to

$$\begin{pmatrix} V_n \\ I_n \end{pmatrix} = \begin{pmatrix} A & B \\ C & D \end{pmatrix} \begin{pmatrix} V_{n+1} \\ I_{n+1} \end{pmatrix} \tag{2.11}$$

Taking in account that the Floquet's Theorem states that the voltages and currents at the n and $n+1$ planes differ only by a propagation factor,

$$V_{n+1} = e^{-\gamma l}\, V_n$$
$$I_{n+1} = e^{-\gamma l}\, I_n \tag{2.12}$$

Now, combining the last expressions (2.11) and (2.12):

$$\begin{pmatrix} V_n \\ I_n \end{pmatrix} = \begin{pmatrix} A & B \\ C & D \end{pmatrix} \begin{pmatrix} V_{n+1} \\ I_{n+1} \end{pmatrix} = \begin{pmatrix} e^{\gamma l} \cdot V_{n+1} \\ e^{\gamma l} \cdot I_{n+1} \end{pmatrix} \tag{2.13}$$

Thus,

$$\begin{pmatrix} A - e^{\gamma l} & B \\ C & D - e^{\gamma l} \end{pmatrix} \begin{pmatrix} V_{n+1} \\ I_{n+1} \end{pmatrix} = 0 \tag{2.14}$$

According to this expression, when the determinant of the matrix is different than zero (being a determined system), it gives trivial solutions. For that reason, the system must be undetermined, which means that the determinant of the matrix must be zero as its represented in the following expression.

$$AD + e^{2\gamma l} - (A + D)e^{\gamma l} - BC = 0 \tag{2.15}$$

As in a reciprocal system $AD - BC = 1$ [6], this expression can be reduced to

$$e^{\gamma l} + e^{-\gamma l} = A + D \tag{2.16}$$

Now, by taking in account that $\gamma = \alpha + j\beta$, and applying the Euler's formula for complex arguments,

$$\cosh(\gamma l) = \frac{A + D}{2} \tag{2.17}$$

As we are considering a lossless and reciprocal periodic structure, $\cosh(\gamma l)$ must be purely real, and in order to accomplish that, $\alpha = 0$ and $\gamma = j\beta$, so the expression can be rewritten as

$$\cos(\beta l) = \frac{A + D}{2} \tag{2.18}$$

In the case where the periodic structure is symmetric and thus, $A = D$, the las expression can be reduced to

$$\cos(\beta l) = A \tag{2.19}$$

This expression corresponds to the dispersion relation of the fundamental harmonic through a unit cell.

2.3 Bloch Impedance

At this point, since the propagating waves in the periodic structure are Bloch waves, it is more convenient to identify the impedance of the transmission lines as Bloch impedances, Z_B [1], which is defined as the relationship between the voltage and the current at any position of the periodic structure.

In order to obtain the expression of the Bloch impedance, it is necessary to introduce the parameter of the relationship between the voltage and current at any position of the periodic structure

$$(A - e^{\gamma l})V_{n+1} + BI_{n+1} = 0 \tag{2.20}$$

which follows that

$$\frac{V_{n+1}}{I_{n+1}} = -\frac{B}{A - e^{\gamma l}}, \quad \forall n \tag{2.21}$$

This last expression is similar to the one of the characteristic impedance of a transmission line as it is defined as the relation between voltage and current for a single propagating wave at any position of the line. At this point, by combining (2.20) and (2.21), the Bloch impedance can be found with two solutions as follows:

$$Z_B^{\pm} = -\frac{2B}{A - D \pm \sqrt{(A + D)^2 - 4}} \tag{2.22}$$

Each solution corresponds to the kind of propagation of the waves. One is for the forward travelling waves and the other one is for the backward travelling waves. As seen previously, the propagation regions are found only when $(A + D)^2 < 4$, when this is being accomplished, the solutions of the expression have the same magnitude and the imaginary part is identical and the real parts have opposite signs. In the band gap regions (the regions where the propagation is not allowed), the solution is purely imaginary with different magnitude.

The imaginary contribution of the solution of the expression (2.22) only exist if the unit cell is asymmetric, in fact, in that case, the imaginary part is not related to the losses, but to the termination of the line. Moreover, when the unit cell is not symmetric (meaning that $A \neq D$), it is possible to distinguish between forward and backward waves (as opposed to case where the unit cell is symmetric) from the point of view of voltage and current waves.

This can be explained as the magnitude of the Bloch impedance is equal in the case of asymmetric unit cell, although it provokes a phase shift between the voltage and current waves.

This can be exposed with the following figure, that represents both cases, the one with a T-circuit symmetric unit cell (vertical dashed lines) and the one with an L-circuit asymmetric unit cell.

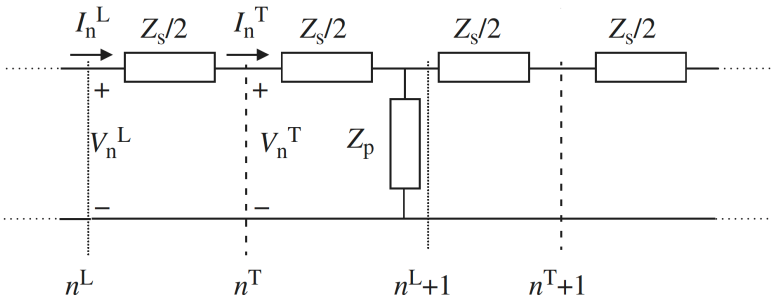

Figure 2.4: Periodic structure representing a symmetric unit cell (vertical dashed lines) and an asymmetric unit cell (vertical dotted lines)

In figure 2.5 in can be seen that $I_n^L = I_n^T$ but, as stated previously, $V_n^L \neq V_n^T$. According to this, it can be understood now the plane shift that provokes that the forward and backward waves can be distinguishable, which is due to the imaginary contribution of the Bloch impedance.

Now, if we take in account the case when the unit cell is symmetric, meaning that $A = D$, the expression (2.22) can be rewritten as

$$Z_B^{\pm} = \pm \frac{B}{\sqrt{A^2 - 1}} \tag{2.23}$$

For the case of a lossless and symmetric structure, the solutions of (2.22) will have opposite signs bust both are real. The sign indicates the propagation of the waves, positive sign for forward travelling waves and negative sign for backward travelling waves.

Since S-parameters are directly related to the ABCD matrix, this expression will be useful at the moment of performing the circuital EM simulations.

Let us consider a periodic structure with symmetric unit cells that can be described by the network of figure 2.4, as it represents a scheme of a periodically perturbed transmission line with symmetric unit cells, implemented by means of loading elements (series and shunt impedances in this case). As stated previously, $A = \cos(\beta l)$, where A corresponds to the dispersion relation. Thus, the elements of the ABCD matrix for the symmetric unit cells from figure 2.4 are:

$$A = D = 1 + \frac{Z_s}{2Z_p} \tag{2.24}$$

$$B = Z_s + \frac{Z_s^2}{4Z_p} \tag{2.25}$$

$$C = \frac{1}{Z_p} \tag{2.26}$$

For the case of the asymmetric unit cell, the parameters would be:

$$A = 1 + \frac{Z_s}{2Z_p} \tag{2.27}$$

$$B = Z_s \tag{2.28}$$

$$C = \frac{1}{Z_p} \tag{2.29}$$

$$D = 1 \tag{2.30}$$

As stated previously, for the asymmetric unit cell case, $A \neq D$, and the dispersion relation is given by

$$\cos(\beta l) = \frac{A+D}{2} = \frac{2+\frac{Z_s}{Z_p}}{2} = 1 + \frac{Z_s}{2Z_p} \tag{2.31}$$

which is the same solution of the dispersion relation in the case of the symmetric unit cell, this means that the position of the reference planes of the unit cell is not important for that expression.

At this point, the equations of the ABCD matrix of the unit cells can be included to the Bloch impedance expression (2.22). First, for the symmetric unit cell, the Bloch impedance is defined as

$$Z_B^{\pm} = \pm \frac{Z_s\left(1+\frac{Z_s}{4Z_p}\right)}{\sqrt{\left(1+\frac{Z_s}{2Z_p}\right)^2 - 1}} = \sqrt{\frac{Z_s}{2}\left(\frac{Z_s}{2}+2Z_p\right)} \tag{2.32}$$

and its solution is real in the propagation regions if Z_s and Z_p are purely reactive impedances. In the case where the unit cell is asymmetric (L-circuit unit cells), the Bloch impedance is defined as

$$Z_B^{\pm} = -\frac{2Z_s}{\left(\frac{Z_s}{Z_p}\right) \pm \sqrt{\left(2+\frac{Z_s}{Z_p}\right)^2 - 4}} = \pm\sqrt{\frac{Z_s}{2}\left(\frac{Z_s}{2}+2Z_p\right)} + \frac{Z_s}{2} \tag{2.33}$$

As mentioned before, the Bloch impedance of an asymmetric unit cell is a complex number in the region where wave propagation is allowed. This means that the imaginary part $Z_s/2$ corresponds to the impedance that must be cascaded to the truncated periodic line and in manifesting the plane shift between symmetric and asymmetric unit cells. Thus, an asymmetric unit cell can have the same behavior as a symmetric unit cell as long as the same reactance is added at the beginning of the structure ($+Z_s/2$ in the source plane) or the opposite reactance is added at the end of the structure ($-Z_s/2$ in the load plane).

3. APPLICATION OF ARTIFICIAL TRANSMISSION LINES BASED ON INDUCTIVE LOADING TO FILTER DESIGN

The idea of this chapter is to explain the steps that have been made during the simulation part of this thesis and also the issues that were found. It will be shown the differences between the ordinary filter and the inductively loaded filter and the reasons why applying this last theory, the filter is much more implementable.

3.1 Specifications and Design of the Ordinary Filter

In order to explain the advantages that the artificial transmission lines can offer, an ordinary filter based on $\lambda/4$ resonators has been designed. As stated previously, these filters are based on the idea that a $\lambda/4$ section of a line that is ended by open circuit or short circuit have the same behavior as an LC circuit in series or shunt, configuration respectively.

As previously mentioned, to realize this study it has been decided to implement the stopband filter, which corresponds to ending the line as an open circuit.

According to the definition of the filter, considering a line section ended by an open circuit (stop band filter), this section of the line will behave as an LC resonator in series only at the frequencies near the operating frequency, for which the line has a length of $\lambda/4$.

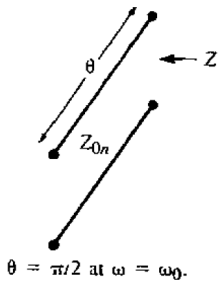

Figure 3.1: Line section of the ordinary filter

In fact, for this line section $Z = -jZ_{on}\cot(\theta)$, where $\theta = \pi/2$ as long as $\omega = \omega_o$. This means that, when the frequencies are near ω_o, or when $\omega = \omega_o + \Delta\omega$,

$$\theta = \frac{\pi}{2}\left(1 + \frac{\Delta\omega}{\omega_o}\right) \tag{3.1}$$

The impedance can be approximated by

$$Z = jZ_{on}\tan\left(\frac{\pi\Delta\omega}{2\omega_o}\right) \approx \frac{jZ_{on}\pi(\omega - \omega_o)}{2\omega_o} \tag{3.2}$$

As it is well known, the impedance of an LC circuit can be expressed as

$$Z = j\omega L_n + \frac{1}{j\omega C_n} = j\sqrt{\frac{L_n}{C_n}}\left(\frac{\omega}{\omega_o} - \frac{\omega_o}{\omega}\right) \approx 2j\sqrt{\frac{L_n}{C_n}}\left(\frac{\omega - \omega_o}{\omega_o}\right) \approx 2jL_n(\omega - \omega_o) \tag{3.3}$$

where $L_nC_n = 1/\omega_o^2$.

Now, as the line section from the figure 3.1 has the same behavior as an LC circuit, the impedances must match, and the only way to obtain this equality between impedances is by verifying that:

$$Z_{on} = \frac{4\omega_o L_n}{\pi} \tag{3.4}$$

The stop band filter corresponding network can be represented as the following equivalent circuit:

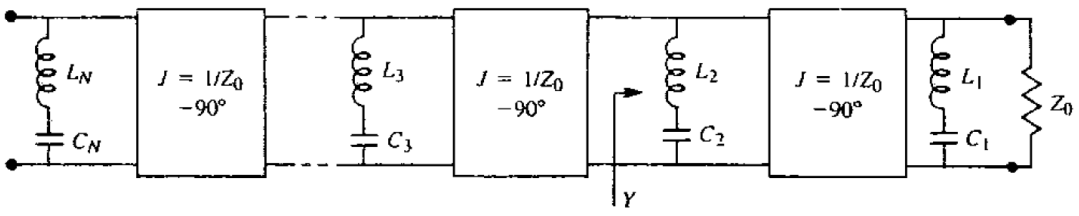

Figure 3.2: Equivalent circuit for the stopband filter

Which, at the same time is equivalent to the following circuit:

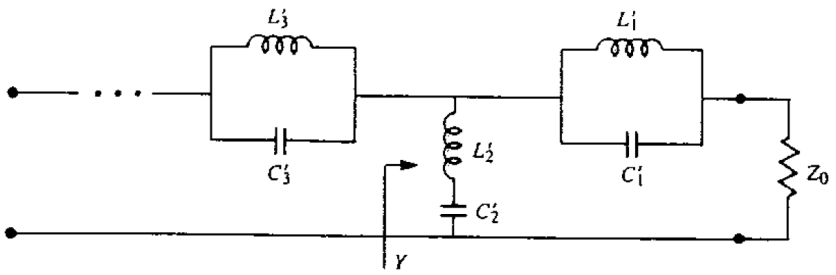

Figure 3.3: Equivalent circuit for the stopband filter

The impedances of these circuits are equivalent only if

$$\frac{1}{Z_o^2}\sqrt{\frac{L_1}{C_1}} = \sqrt{\frac{L_1{}'}{C_1{}'}} \quad ; \quad \sqrt{\frac{L_2}{C_2}} = \sqrt{\frac{L_2{}'}{C_2{}'}} \tag{3.5}$$

From which the following relations can be obtained

$$\mathrm{L}_1 = \frac{Z_o^2}{\omega_o^2 L_1} \; ; \quad L_2 = L_2{}' \tag{3.6}$$

And finally, by applying the relation of $L_n C_n = L_n' C_n' = 1/\omega_o^2$, and from the expression (3.6) and the impedance scaling and frequency transformations, the following expression can be obtained

$$Z_{on} = \frac{4Z_0}{\pi g_n \Delta} \tag{3.7}$$

where Δ corresponds to the relative bandwidth, Z_0 is the characteristic impedance of the host line, g_n are the elements of the low-pass filter prototype and Z_{on} the characteristic impedance of the stubs that will be used to calculate the impedances of the five stubs.

As mentioned before, the filter response that will be implemented is the Chebyshev 0.5dB ripple response, which corresponds to the following table:

0.5 dB Ripple

N	g_1	g_2	g_3	g_4	g_5	g_6	g_7	g_8	g_9	g_{10}	g_{11}
1	0.6986	1.0000									
2	1.4029	0.7071	1.9841								
3	1.5963	1.0967	1.5963	1.0000							
4	1.6703	1.1926	2.3661	0.8419	1.9841						
5	1.7058	1.2296	2.5408	1.2296	1.7058	1.0000					
6	1.7254	1.2479	2.6064	1.3137	2.4758	0.8696	1.9841				
7	1.7372	1.2583	2.6381	1.3444	2.6381	1.2583	1.7372	1.000			
8	1.7451	1.2647	2.6564	1.3590	2.6964	1.3389	2.5093	0.8796	1.9841		
9	1.7504	1.2690	2.6678	1.3673	2.7239	1.3673	2.6678	1.2690	1.7504	1.0000	
10	1.7543	1.2721	2.6754	1.3725	2.7392	1.3806	2.7231	1.3485	2.5239	0.8842	1.9841

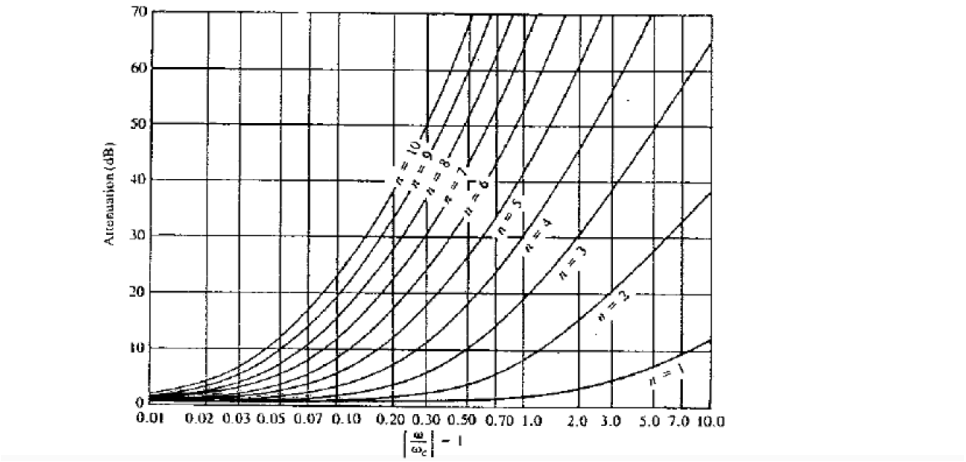

Figure 3.4: Element values for Equal-Ripple Low-Pass Filter Prototypes

Knowing that the characteristic impedance of the host line $Z_0 = 50\Omega$ and the relative bandwidth $\Delta = 0.3$, the different characteristic impedances of the stubs Z_{on} can be found as:

Z_{o1}	124.4Ω
Z_{o2}	172.6Ω
Z_{o3}	83.5Ω

And as $g_4 = g_2$ and $g_5 = g_1$, the impedances $Z_{o4} = Z_{o2}$ and $Z_{o5} = Z_{o1}$

Once this has been calculated, the ideal ordinary filter schematic can be obtained as shown in figure 3.5.

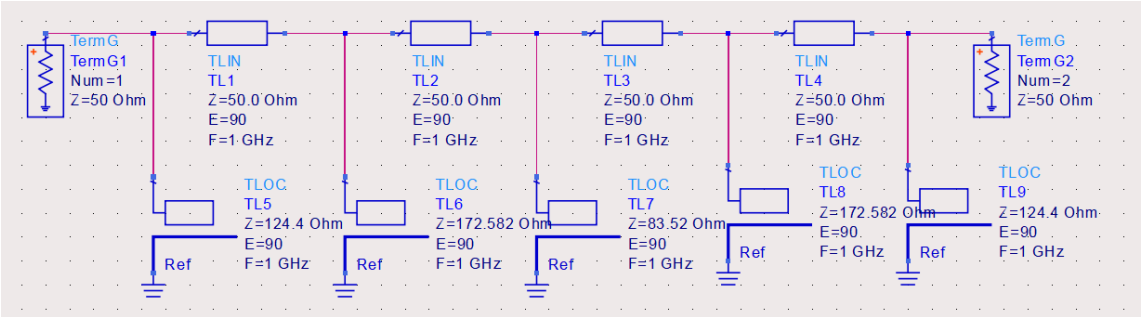

Figure 3.5: Ideal Ordinary Filter Design

The host line is composed by four identical transmission line sections with characteristic impedance $Z_0 = 50\Omega$ and with electrical length 90º. The stubs have also an electrical length of 90º and each line corresponds to the impedance calculated previously.

The response of this circuit is represented in figure 3.6, where it can be seen, as expected, that the transmission coefficient S_{21} at the frequency of operation of 1GHz is practically null, as it corresponds to a stopband filter and no transmission is wanted at the frequency of operation, and, on the contrary, the reflection coefficient S_{11} is very close to 0dB.

As the bandwidth has been determined to 30%, the range of the stopband starts at 850MHz and ends at 1150MHz as shown in figure 3.6.

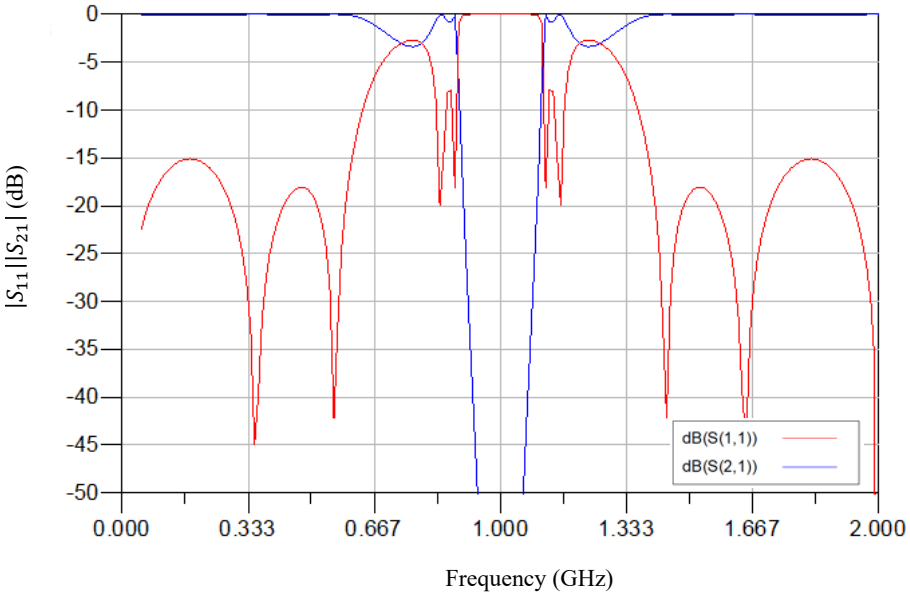

Figure 3.6: Ideal Ordinary Filter Response

At this point, the substrate must be defined in order to implement the filter according to the substrate conditions. For this case, the substrate that has been decided to implement the filter is ROGERS RO3010 with dielectric constant $\varepsilon = 10.2$, loss tangent $tan\delta = 0.0023$, thickness $h = 1.27mm$ and thickness $t = 35\mu m$. The reason why this is the substrate that has been determined is because it is a very common and cheap substrate, very easy to obtain and to work with.

By generating the previously calculated impedances with this substrate, it is observed that the values of the widths of these impedances are very small, such so, that it is impossible to implement it physically. As it is shown in the figure below, the widths of the impedances go from $1.3\mu m$ to $273\mu m$. Usually, lines bellow $200\mu m$ are not implementable within this substrate.

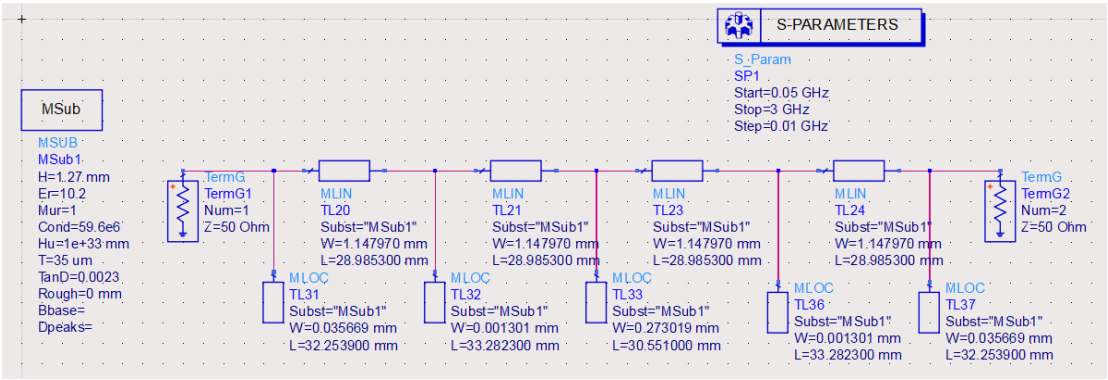

Figure 3.7: Ordinary Filter Design with substrate

Therefore, the response of this simulation is being affected by this size problem and it does not behave as expected.

This is the main reason why the application of artificial transmission lines based on inductive loading to this filter is very useful. In order to be able to implement physically a filter of that kind without modifying it by loading it with reactive elements, the bandwidth would have to be incremented much more, as the values of the impedances are inversely proportional to it, as shown in expression (3.7).

3.2 Filter Design Based on Artificial Lines with Inductive Loading

Once the main reason of the realization of this study has been exposed, the design of the filter based on artificial transmission lines with inductive loading will be detailed.

It has been decided that these techniques will only be applied on the stubs, as there is no implementation problem according to the host line.

In the previous chapter, the T-circuit model has been introduced in figure 2.6 as it can explain very well the concept of the unit cell, it has also been seen that the symmetric unit cell has much more simpler equations that the asymmetric unit cell, therefore, it has been decided to use a symmetric unit cell provided by the equivalent T-circuit model as the reference design that will be inserted at the stubs of previously presented ordinary filter.

Moreover, one important fact that was stated on the previous chapter, is that the series and shunt impedances of the unit cell must be reactive impedances, this way the Bloch impedance will have a real solution. Let us discuss about the kind of reactive impedance, either shunt capacitors or series inductors, that will be inserted in the artificial transmission lines of the stubs of the filter, in order to implement the most efficient design.

In order to have a better understanding of the two possible T-circuit models for a single unit cell, the representation in figure 3.8 presented.

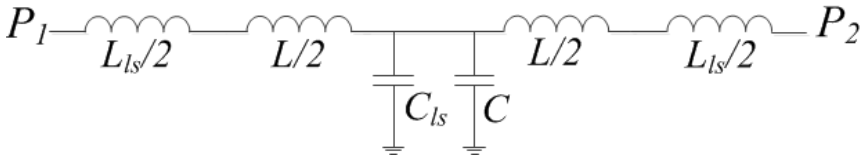

Figure 3.8: Capacitively-loaded and inductively-loaded unit cell

The L and C components are modelling the characteristic parameters of the ordinary transmission line such as Z_0 (with an electrical length kl), while L_{ls} and C_{ls} correspond to the reactive loading elements that define the unit cell, which, by repeating it periodically, it will define the artificial transmission line.

It is well known that the characteristic impedance of a transmission line is

$$Z_0 = \sqrt{\frac{L}{C}} \tag{3.8}$$

Now, due to the periodicity of the unit cells, a Bloch wave is going to be appeared, and consequently, the concept of Bloch impedance must be taken into account. At this point, the Bloch impedance can be represented as:

$$Z_B = \sqrt{\frac{L + L_{ls}}{C}} \tag{3.9}$$

for the case of introducing series inductors as the reactive element, and

$$Z_B = \sqrt{\frac{L}{C + C_{ls}}} \tag{3.10}$$

for the case of introducing shunt capacitors as the reactive element.

As it can be seen in the previous equations (3.9) and (3.10), for the case of loading the line with series inductors, the characteristic impedance of the ordinary line will be reduced. And, in counterpart, for the case of a loading periodically with shunt capacitors, the opposite will occur.

Moreover, these expressions are approximations and are only applicable when working at very low frequencies. For this reason, later on, the more accurate expression for the Bloch impedance will be introduced.

As mentioned in the first section of this chapter, the main problem of the implementation of the ordinary filter is that the value of the characteristic impedances of the stubs is too high and, therefore, the lines are too narrow, being unable to implement. For that reason, the design of the stubs of the filter will be carried out by means of inductively-loaded artificial transmission lines.

At this point, it is necessary to know how to obtain the different values of the introduced parameters. There are two design equations:

$$\cos(\beta l) = \cos(kl) - \frac{\omega}{2} \cdot \frac{L_{ls}}{Z_0} \sin(kl) \tag{3.11}$$

$$Z_B = \frac{1}{\sin(\beta l)}\left\{L_{ls} \cdot \omega \cdot \cos(kl) + \left(Z_0 - \frac{L_{ls}^2}{4} \cdot \frac{\omega^2}{Z_0}\right) \cdot \sin(kl)\right\} \quad (3.12)$$

where βl and kl are the electrical lengths of the loaded and unloaded transmission lines, respectively. The inductance L_{ls} corresponds to the reactive loading element that will be in the unit cell, which will be repeated along the line, constituting the artificial transmission line.

These equations have three unknown parameters which are Z_0, kl and L_{ls}. Therefore, there is one more equation needed to achieve a solution for these parameters, this last equation corresponds to the slow wave ratio, which will determine the degree of miniaturization from an unloaded transmission line compared to a loaded line, while having the same electrical length. This ratio can be represented as follows

$$swr = \frac{v_{pl}}{v_{po}} = \frac{\omega/\beta}{\omega/k} = \frac{kl}{\beta l} \quad (3.13)$$

As stated previously, by periodically loading the line with inductances, significant dispersion, pass bands and stop bands appear, and the phase velocity of the line is reduced. This slow-wave effect is interesting to reduce the size of microwave components in general.

The slow wave ratio that has been decided to apply is 0.5, as it allows to reduce the size of the line to the half approximately. This is a reasonable value for swr, as defining a too small value will increase the value of the inductances, and the layout design of those inductances will have to be narrower. As the layout design of these inductances have already been designed using the technology limits in terms of width, in order to increase them, its layout design would have to be longer, therefore, the size of the whole structure would be increased. There is always a trade-off in the choice of this parameter.

Another important fact is the number of unit cells that will be introduced in the periodically loaded structure, this number is defined as N. This parameter has been finally specified to $N = 3$ after realizing a few tests in order to find the most suitable option for this study.

As mentioned before, the reactive loading of the unit cells will be carried out by means of inductances. Thus, the unit cell will have the following form:

Figure 3.9: Unit cell of the filter

At this point, once the design equations have been determined and the input parameters defined, it is possible to find the design parameters by applying the previously mentioned equations (3.11), (3.12) and (3.13)

It has been observed that implementing it with only one or two stages, the impedances still being too high in order to its physical implementation.

For the case where $N = 1$, it has been observed that the impedances of the stubs still being too high. In the following table the parameters for that case are shown:

Input Parameters							
f_0	N	swr	βl	kl	Z_{B_1}	Z_{B_2}	Z_{B_3}
$1GHz$	1	0.5	$\frac{\pi}{2}$	$\frac{\pi}{4}$	124.4Ω	172.58Ω	83.52Ω

Table 3.1: Input Parameters of the unit cell with $N = 1$

Unknown Parameters					
Z_{0_1}	Z_{0_2}	Z_{0_3}	L_{ls_1}	L_{ls_2}	L_{ls_3}
87.96Ω	122Ω	59Ω	$14nH$	$19.4nH$	$9.39nH$

Table 3.2: Output Parameters of the unit cell with $N = 1$

Only the impedances Z_{0_1}, Z_{0_2} and Z_{0_3} are shown as $Z_{0_4} = Z_{0_2}$ and $Z_{0_5} = Z_{0_1}$. It can be seen that the value of these impedances have been reduced by applying the artificial

transmission lines technology, loading the line inductively. Although, these values of impedances are still too high in order to implement them with the desired substrate.

At this point, it is necessary to check the possibility of implementing it with $N = 2$. For that case, the solutions of the previous mentioned equations (3.11), (3.12) and (1.3) are the following:

Input Parameters							
f_0	N	swr	βl	kl	Z_{B_1}	Z_{B_2}	Z_{B_3}
$1GHz$	2	0.5	$\frac{\pi}{4}$	$\frac{\pi}{8}$	124.4Ω	172.58Ω	83.52Ω

Table 3.3: Input Parameters of the unit cell with $N = 2$

Unknown Parameters					
Z_{0_1}	Z_{0_2}	Z_{0_3}	L_{ls_1}	L_{ls_2}	L_{ls_3}
67.3Ω	93.4Ω	45.2Ω	$37.82nH$	$52.9nH$	$25.4nH$

Table 3.4: Output Parameters of the unit cell with $N = 2$

In order to evaluate if these solutions are implementable, it must be known that the maximum value of impedance that can be implemented within the desired substrate is about 90Ω, which corresponds to a width of the line of $200\mu m$.

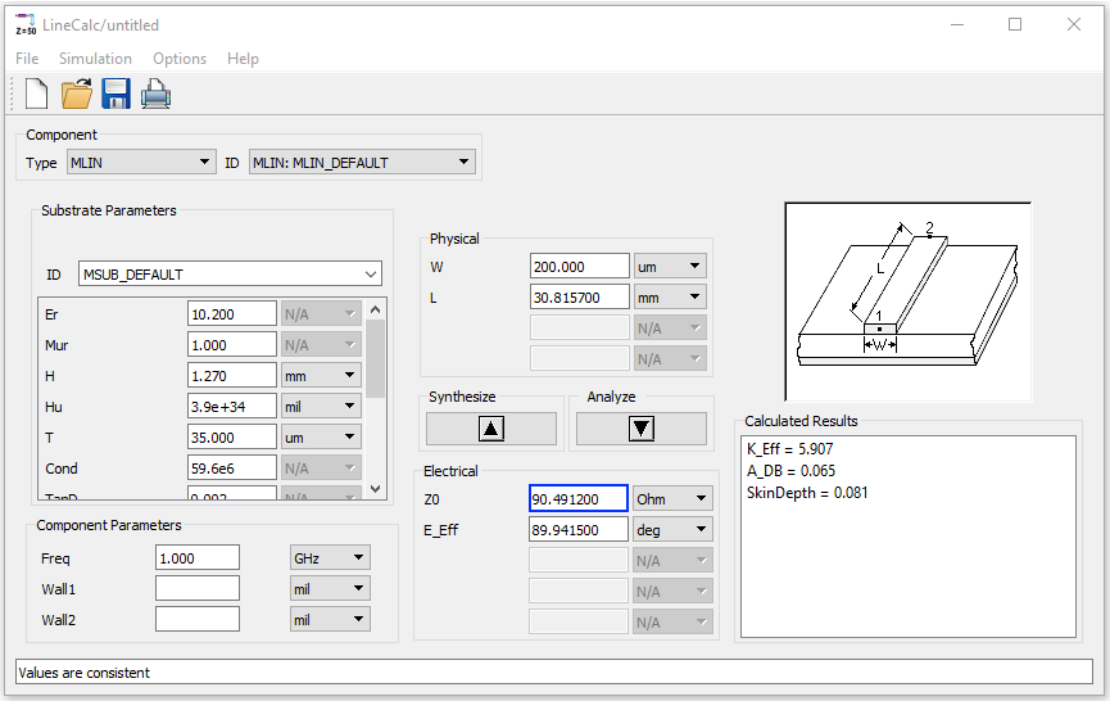

Figure 3.10: LineCalc image showing the maximum allowed impedance

Moreover, it can be seen that the biggest impedance is the one corresponding to the second stub, Z_{0_2} (and consequently Z_{0_4}). For that case of introducing two unit cells at the line, this impedance is higher than the limit stablished by the substrate, therefore it is not possible to implement the filter with this structure.

On the other hand, it must be also taken into account the value of the inductances that are going to be loaded to the line. Later on, it will be seen that if this value is too high, it can be difficult to implement the inductance in planar microstrip technology.

Finally, the case of introducing three stages of the unit cell at the line has been taken in account.

Input Parameters							
f_0	N	swr	βl	kl	Z_{B_1}	Z_{B_2}	Z_{B_3}
$1GHz$	3	0.5	$\frac{\pi}{6}$	$\frac{\pi}{12}$	124.4Ω	172.58Ω	83.52Ω

Table 3.5: Input Parameters of the unit cell with $N = 3$

Unknown Parameters					
Z_{0_1}	Z_{0_2}	Z_{0_3}	L_{ls_1}	L_{ls_2}	L_{ls_3}
64.4Ω	89.33Ω	43.23Ω	$3.95nH$	$5.48nH$	$2.66nH$

Table 3.6: Output Parameters of the unit cell with $N = 3$

The results when $N = 3$ seem much more optimal as al the impedances have values below the technology limit of 90Ω.

This is why it has been finally decided to implement the artificial transmission lines to the stubs of the filter using 3 stages. Using a too large number of stages can cause too small impedances, therefore, this number of stages seem the most suitable for this filter.

This means that the design is finally composed by three unit cells of $\beta l = \pi/6$ each one and a slow wave ratio of 0.5. These assumptions seem the most proper ones, from an analytical point of view.

As mentioned previously, the artificial transmission lines theory will only be applied to the stubs of the filter, therefore, as there are three different stubs (as the order of the filter is 5 and $Z_{o4} = Z_{o2}$ and $Z_{o5} = Z_{o1}$), three different artificial transmission lines will be generated.

The following figures show the three different artificial transmission lines that have been generated in order to substitute the ordinary lines of the stubs of the filter. The first stub, which originally had an impedance of 124.4Ω and wasn't implementable, has been replaced by periodically inductively-loaded line using three unit cells where the new impedance is 64.4Ω and the value of the inductances is $3.95nH$. This artificial transmission line should have the exact same behaviors at the frequency of operation than the original line of 124.4Ω.

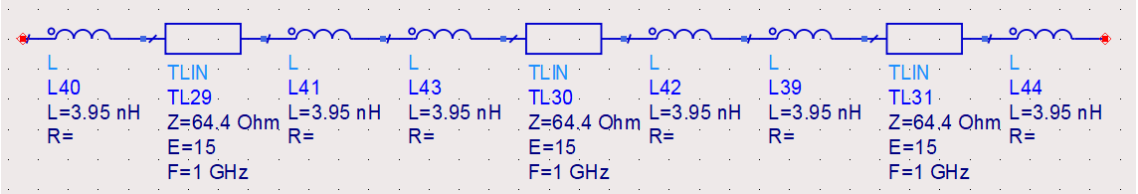

Figure 3.11: Artificial transmission line of the first stub

It can be observed that the second line has the highest values for both, impedance and inductance, although, the impedance value, 89.33Ω, is below the technology limit. Therefore, at a first sight, that doesn't seem a big issue.

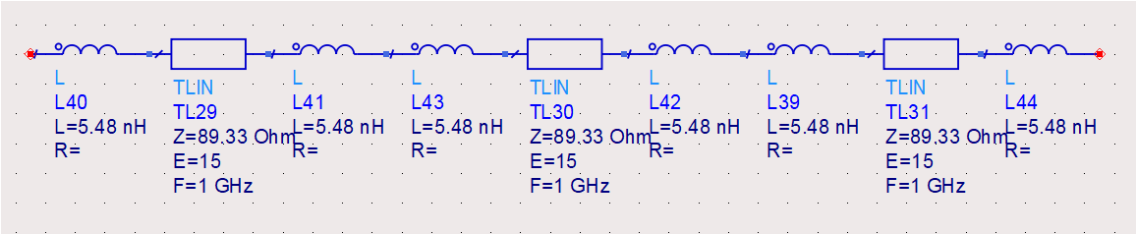

Figure 3.12: Artificial transmission line of the second stub

Finally, the third stub is the one corresponding to the lowest inductances and impedances. Apparently, this stub seems to be the easiest one in order to generate the physical design, as, the smallest the inductances, the easier it is to implement them using planar microstrip technology. This will be seen properly on the next chapter.

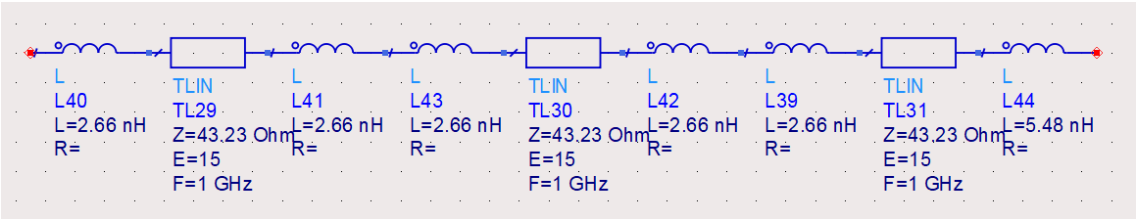

Figure 3.13: Artificial transmission line of the third stub

Once the design of the artificial transmission lines of the stubs have been carried out, the complete circuital model of the filter can be implemented by following the topology of figure 1.1. The proposed architecture of the filter can be seen in figure 3.14.

Notice that it is composed by means of a host line composed by four 90º lines and five cascaded 90º stubs each ended with open circuit; therefore, it is not necessary to add the final inductance of the last unit cell.

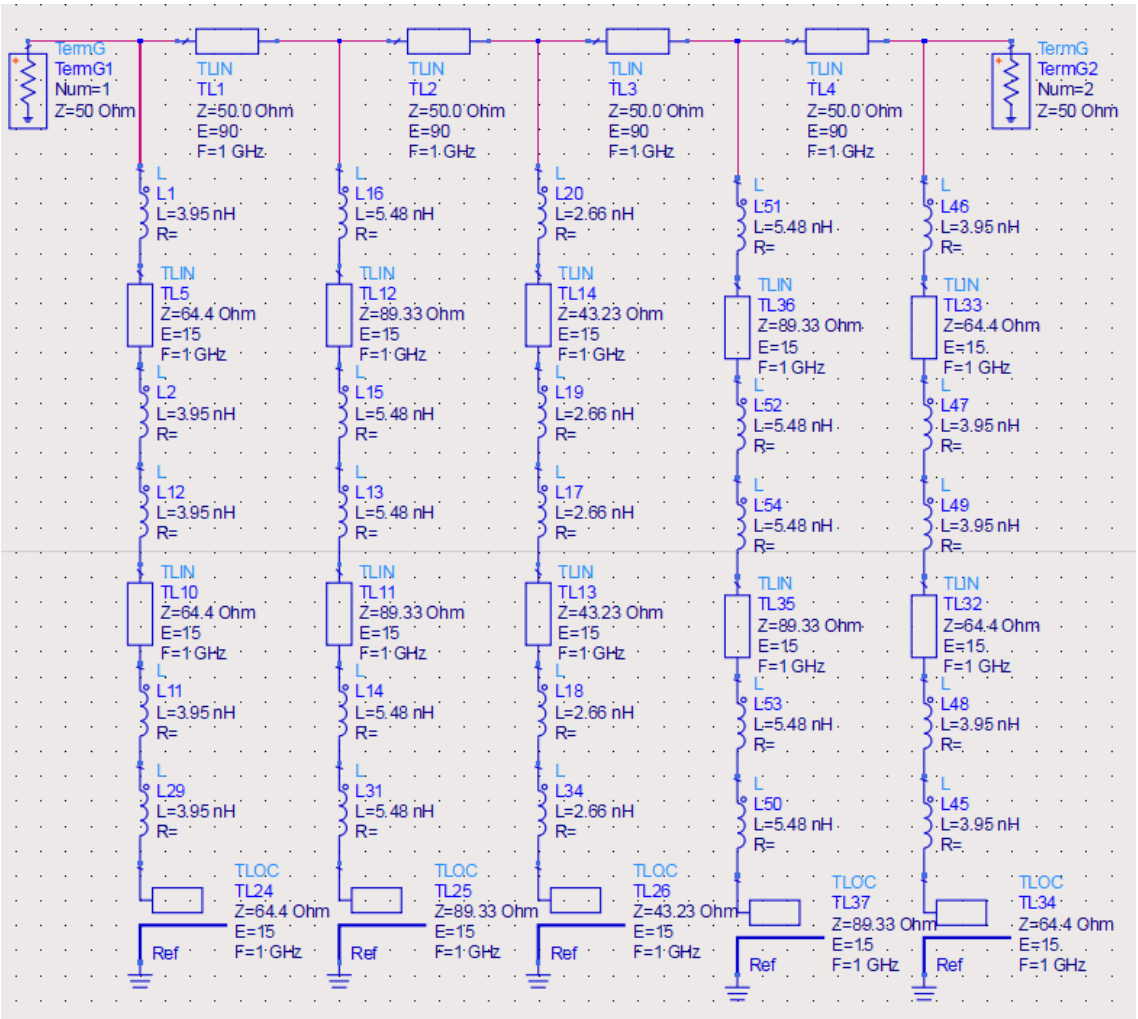

Figure 3.14: Ideal circuit model for the filter by means of artificial transmission lines with inductive loading

By loading the filter inductively it has been achieved smaller values of the impedances and, therefore, higher widths that go from $210\mu m$ to $1.54mm$, meaning that it is now possible to implement the filter physically as the widths of the lines are all above the technology limit, which is, as mentioned before, $200\mu m$ minimum width.

Now, let us represent the response of this filter in terms of the reflection and transmission coefficients. It can be seen that, as expected, the response of this filter generates a stopband on the operating frequency of 1GHZ.

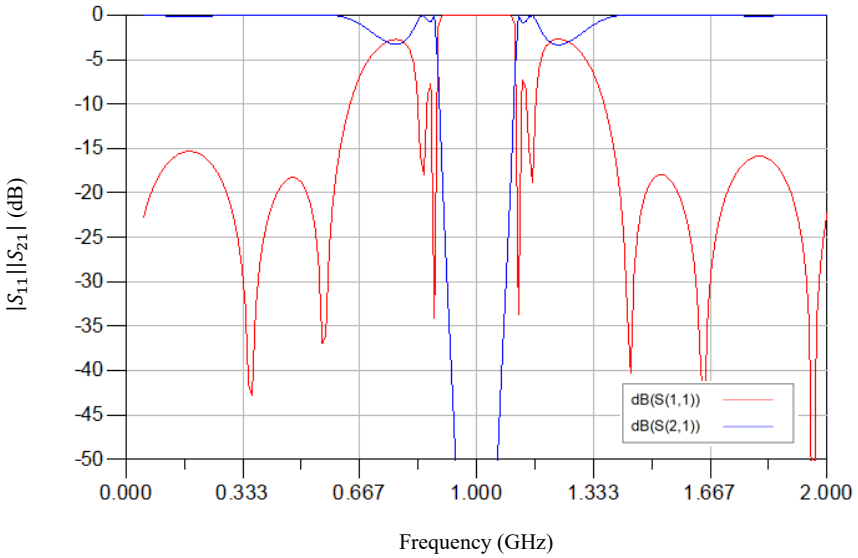

Figure 3.15: Filter based on artificial transmission lines with inductive loading response

This demonstrates that the artificial transmission lines seem to be a useful method to use in order to implement this kind of filter. Later on, it will be seen the comparisons between the convectional filter with the loaded filter.

At this point, the response of the ordinary filter and the inductive loaded filter will be compared in order to verify that loading the lines of the ordinary filter inductively do not have any effect on its response, and both, the frequency of operation and bandwidth are the desired ones.

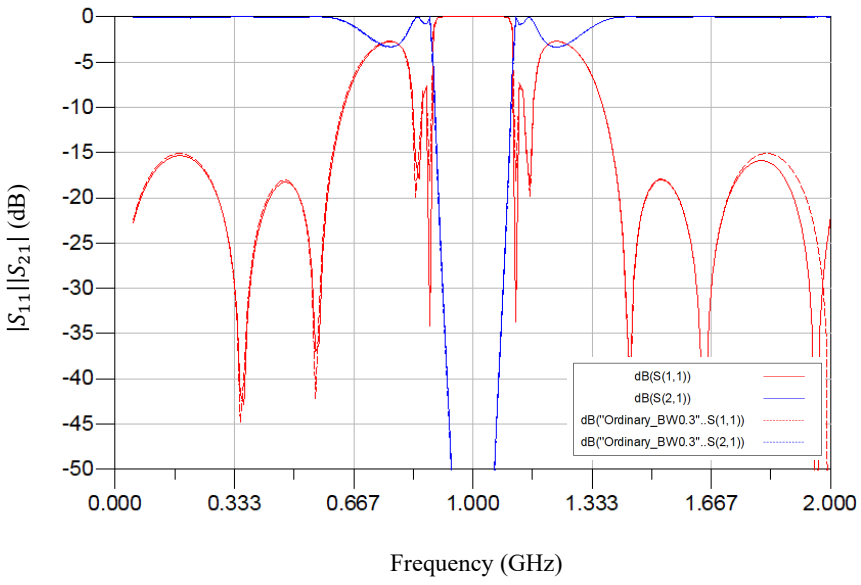

Figure 3.16: Comparison between Ordinary and Inducted Loaded filters

Notice that, in figure 3.16, the result obtained by applying the artificial transmission lines to the stubs, is exactly the same compared to the ordinary filter at the region of interest and the bandwidth also matched the desired 30% specified previously.

4. PHYSICAL DESIGN

At this point, now that the circuital model of the filter based on artificial lines with inductive loading has been performed successfully, let us start its layout implementation in planar microstrip technology using ADS Momentum.

4.1 Physical Design of the Inductances

The layout design of the loading inductors is a bit complex. A transmission line has both, inductive and capacitive effects so, one option to enhance the inductive effect, is to reduce the width of the transmission line in order to reduce the capacitive effect between the strip and the ground plane. This width reduction has the limit of the $200\mu m$ that was stated previously. Therefore, the only option to generate the inductors is to lengthen the strip until achieving the desired inductive effect.

The procedure followed to implement the loading inductors consists in achieving the same reactance than an ideal $L_{ls}/2$ provides at 1 GHz with the proposed layout design. So, first of all, the inductor will be designed and compared with the ideal inductor, later on, the host line will be added and, finally, according to the unit cell configuration, the same inductor will be added to the structure. The inductors have been meandered in order to not increase too much the size of the filter.

The main problem of this procedure is that, by adding the inductors to the line, it is being introduced a phase shift to the whole line, so, this phase shift must be compensated by reducing the impedance values of the lines. The greater number of unit cells, the more phase shift appears.

As stated before, there are three different stubs, in figure 4.1 it is shown the inductance of the artificial transmission line of first stub, which corresponds to $L_{ls_1} = 3.95nH$.

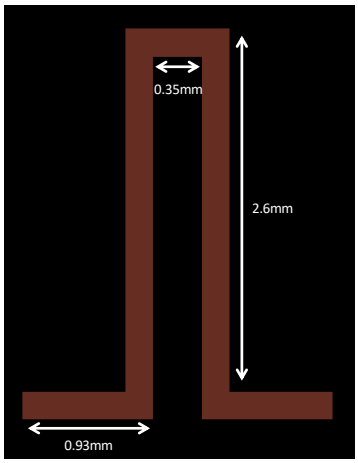

Figure 4.1: Layout design of the inductance of the first stub

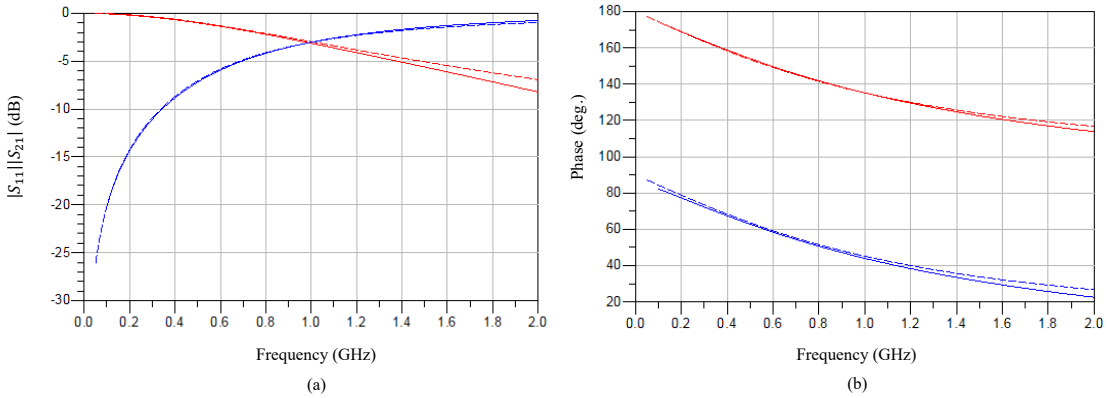

Figure 4.2: Layout and schematic comparison of response (a) and phase (b) of the inductance of the first stub

In figure 4.2, a comparison has been made between the ideal inductor of the schematic and the layout of the inductor of the first stub. It can be seen that both, the responses and the phases, are almost the same in the region of interest.

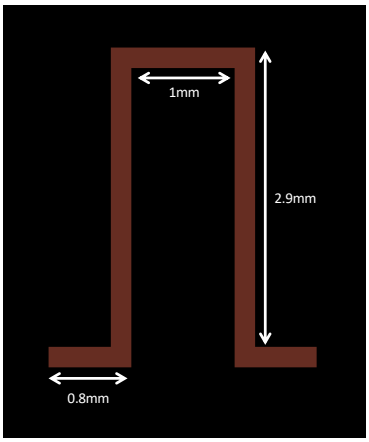

Figure 4.3: Layout design of the inductance of the second stub

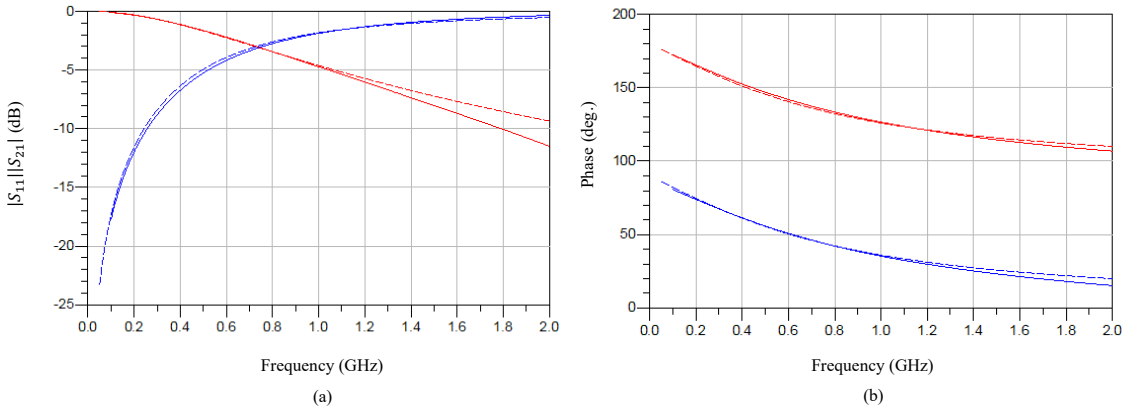

Figure 4.4: Layout and schematic comparison of response (a) and phase (b) of the inductance of the second stub

The inductance from the second artificial transmission line stub is the one corresponding to a very high value of $L_{ls_2} = 5.48nH$. The layout is shown in figure 4.3, where it can be appreciated that this inductance is a bit bigger than the one corresponding to L_{ls_1}. Figure 4.4 demonstrates that the layout design of this inductance corresponds to the schematic inductance.

Finally, the third inductance ($L_{ls_3} = 2.66nH$) is represented in figure 4.5 where it can be appreciated that it is the smallest one as its value corresponds also to the lowest one of the three different inductances.

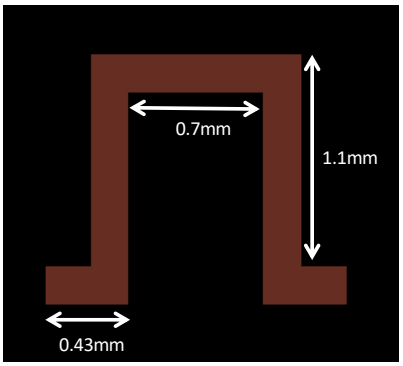

Figure 4.5: Layout design of the inductance of the third stub

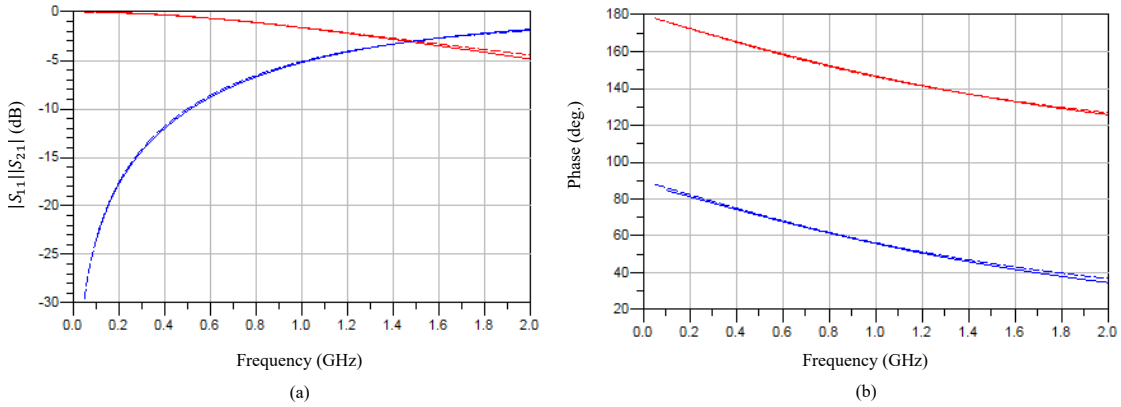

Figure 4.6: Layout and schematic comparison of response (a) and phase (b) of the inductance of the third stub

Once the inductances have been designed, the lines with the mentioned impedances have been added to the structure, following the configuration of the unit cell, until the stubs have been generated by means of three unit cells. As stated previously, the stubs must be ended with open circuit (as it corresponds to a stopband filter), for that reason, in the last unit cell of each stub, the inductor is not added, as it won't introduce any effect.

4.2 Physical Design of the Filter

At this point, now that the inductors of each stub have been designed and the impedances are known, the layout of the three stubs can be designed. In order to generate the layout of the stubs, it must be taken into account the previously mentioned phase shift added by the inductances. Therefore, the length of the lines is going to be reduced in order to compensate it. Moreover, the length of the inductors is going to be also adjusted. Finally, the layout design of the stubs is shown in figures 4.7, 4.9 and 4.11.

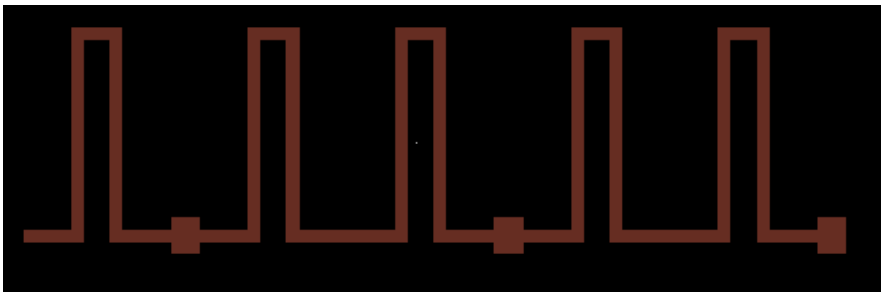

Figure 4.7: Layout of the artificial transmission line of the first stub

In order to check if this unit cell layout design achieves the desired behavior, its frequency response and phase have been compared to the ideal circuital model of this stub.

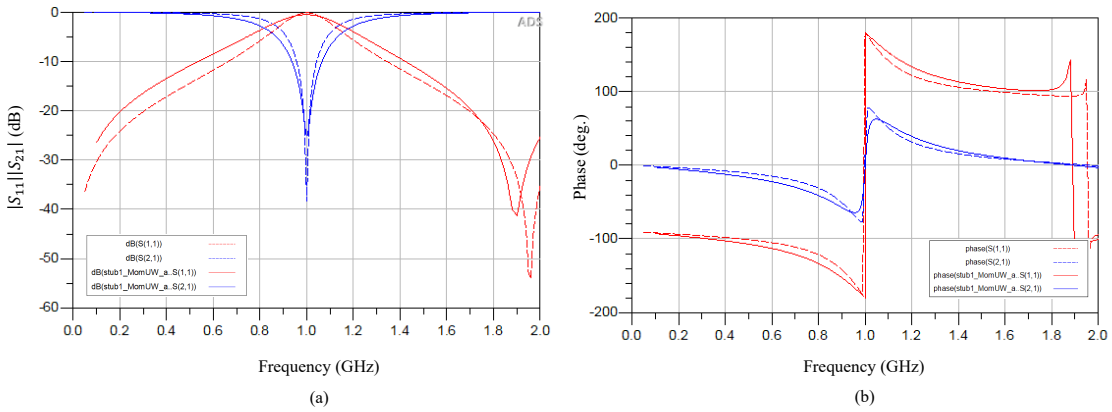

Figure 4.8: Frequency response (a) and phase (b) comparison of the first stub

It can be observed that the phase has been adjusted and at the frequency of operation of 1GHz, the responses are very similar, although, once we take a look at the whole bandwidth, it can be seen that the responses differ a bit more.

For the case of the second stub, which is the one with the highest value of the inductance, it can be evident that these inductors will be the ones that add more phase shift to line. Moreover, the impedances of these stubs are the ones with the highest value, for that reason, the lines of these impedances are very thin. The final implementation of the second stub is represented in figure 4.9, where it can be seen that the lines that are in between the inductors are very small in order to compensate the phase shift introduced by the inductors.

Figure 4.9: Layout of the artificial transmission line of the second stub

Once comparing the response of the layout and the schematic of the stub, the response represented in figure 4.10 is obtained. In the figure, it can be seen that the response is not as precise as in the first stub, this may be because of the high values of the inductors. By adding the components of the artificial transmission line one by one, it has been every time more complicated to adjust it.

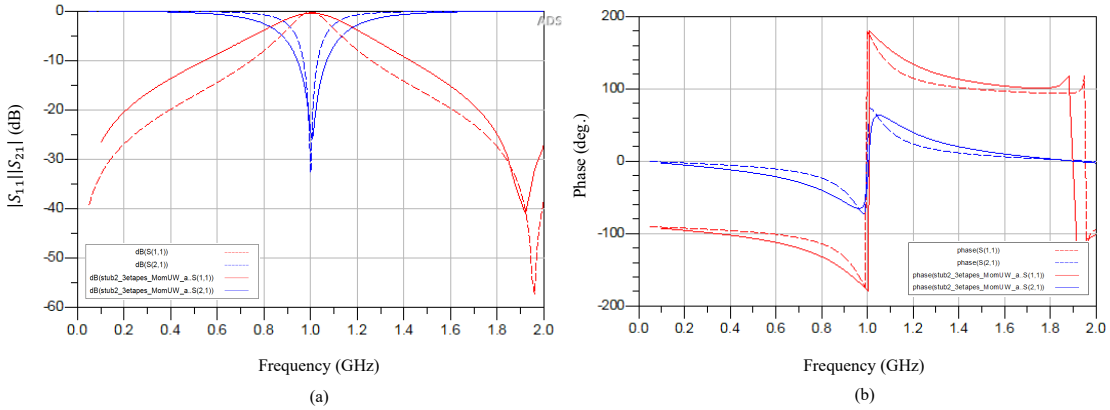

Figure 4.10: Frequency response (a) and phase (b) comparison of the second stub

The response of the second stub is not as accurate as the one from the first stub, even though, at the frequency of operation it seems that it behaves properly.

Finally, the third stub have been designed. This stub is the one with the lowest value of inductances and impedances, so, it has been the easiest one to design, as the phase shift added by the inductances was very low.

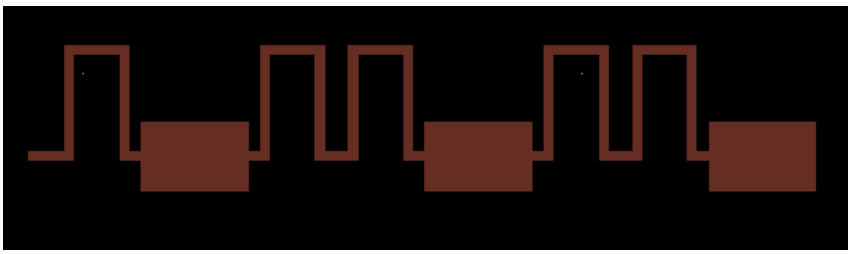

Figure 4.11: Layout of the artificial transmission line of the third stub

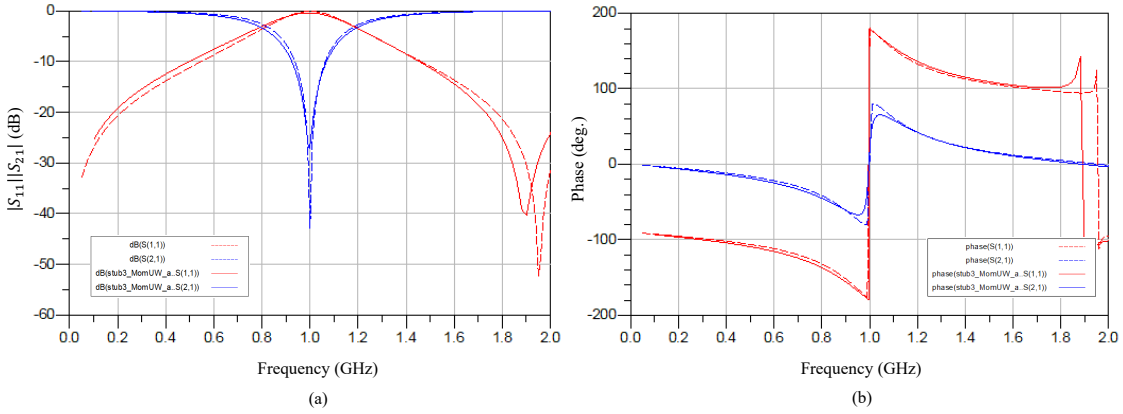

Figure 4.12: Frequency response (a) and phase (b) comparison of the third stub

As expected, the response and the phase of the layout of this stub is the most accurate one compared to the circuital model of the stub. Not only at the frequency of operation, but also at the whole bandwidth.

Once the three stubs have been designed and checked that the behavior of each is the most accurate one, it is the moment to implement the layout of the filter. The final layout design of the filter is represented in figure 4.13.

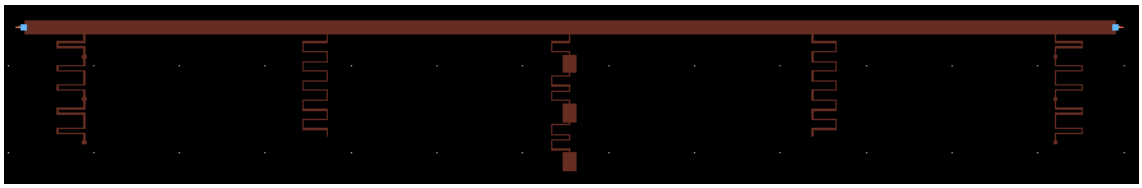

Figure 4.13: Stopband filter layout by means of artificial transmission lines

Notice that the first and the second stubs are repeated at the end of the filter in order to make it symmetric and knowing that $Z_{o4} = Z_{o2}$ and $Z_{o5} = Z_{o1}$ according to (3.7), while the third stub it's only at the center of the filter.

The final design of each stub had to be also adjusted once it was all implemented in the design (except for the width of the inductances, which was established to the technology limit of $200\mu m$) in order to have the better response as possible. The final sizes of each unit cell of the stubs are shown in figures 4.14, 4.15 and 4.16.

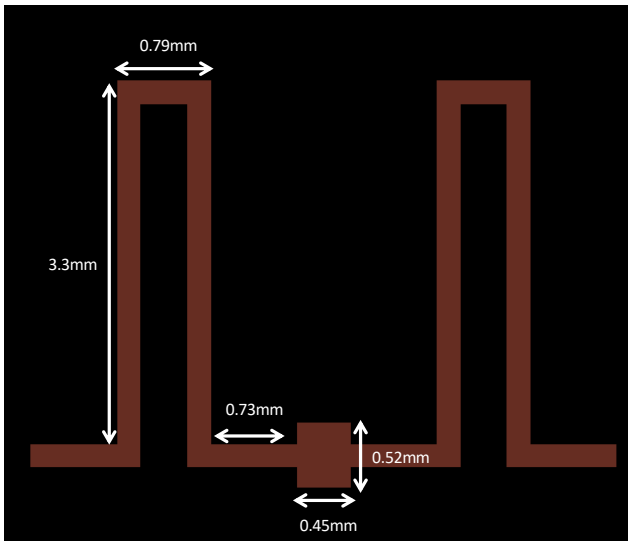

Figure 4.14: Unit cell of the first stub

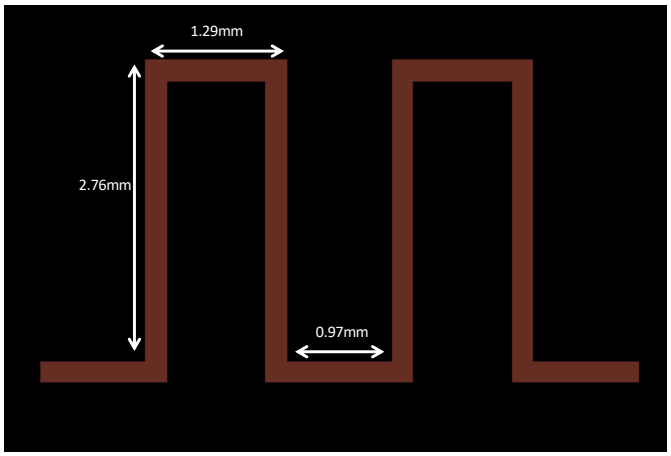

Figure 4.15: Unit cell of the second stub

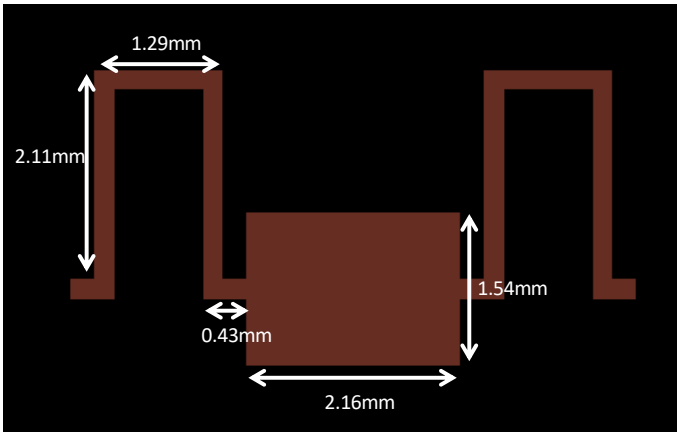

Figure 4.16: Unit cell of the third stub

Now, let us represent the results of the EM simulation of the filter compared to the schematic in figure 4.17 to see the frequency response of the transmission coefficient S_{21}.

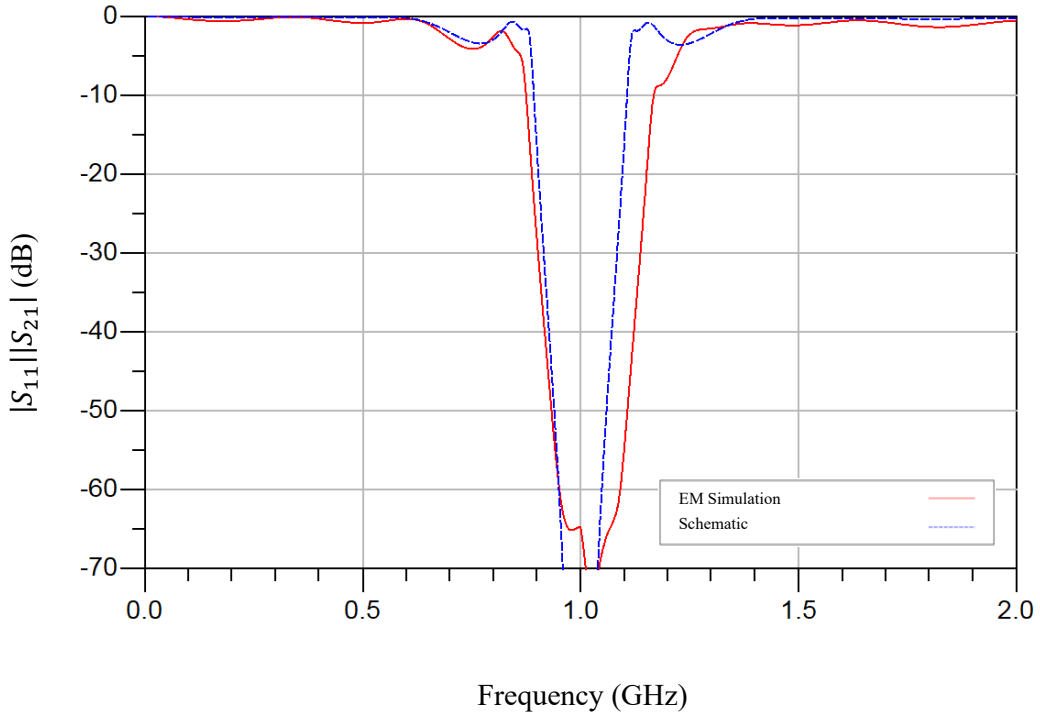

Figure 4.17: S_{21} response of the filter layout with artificial transmission lines compared to schematic

As it can be seen, the designed filter at the frequency of operation of 1GHz has substantially no transmission as S_{21} is around -64dB. Although, it is true that the bandwidth is a bit higher than the original one of 30% and the new bandwidth corresponds to a 40%. This is probably due to the bandwidth discrepancies that were seen when designing the stubs (mostly with the first and the second stubs), where, as mentioned before, the values of the inductances were very high and therefore, there was an important phase shift introduced by the inductances to the line.

In the frequency response of S_{11} (shown in figure 4.18), the same bandwidth disagreement can be observed between the schematic and layout of the filter, although, as expected, the reflection coefficient in the operating frequency is near to one.

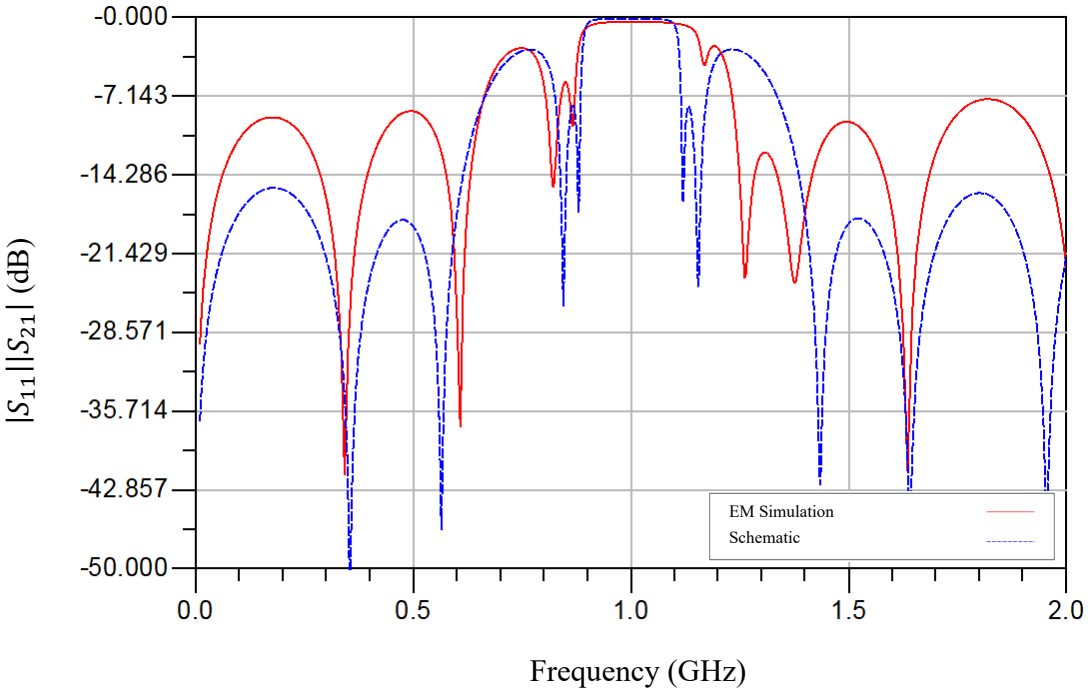

Figure 4.18: S_{11} response of the filter layout with artificial transmission lines compared to schematic

As this bandwidth disagreement seems to be due to the high value of the inductances, a solution to this problem that might be reasonable would be to try to reduce its value. For this reason, it has been decided to implement de second stub with $N = 4$ instead of $N = 3$ as it is the stub with the highest value of inductance and with the worst response in terms of bandwidth, as it can be seen in figure 4.10, that comparing it with 4.8 or 4.12, the EM simulation of this stub is the one that differs more from the schematic version of the stub. The other stubs have been left with $N = 3$ as this has been done only to check if this is a good solution and might not result into any better response of the filter.

At this point, the second stub has been redesigned completely, as all the parameters change now that it is being implemented with $N = 4$. As shown in table 3.6, as input parameters to calculate the new ones, there are βl, swr and Z_{B_2}, which are exactly the same as for generating the stub with $N = 3$. According to equations (3.11) and (3.12), the new parameters of the second stub are $Z_{0_2} = 88\Omega$ and $L_{ls_2} = 4.08nH$.

The new values of Z_{0_2} and L_{ls_2} seem to be reasonable in order to implement the stub, as the new impedance value is still implementable according to this technology and substrate and the new inductance is much lower than the previous one.

The layout of the new stub has been designed in order to check if this is really a good solution for the bandwidth problem. It can be seen in figure 4.19 that in this new case, the unit cell is repeated 4 times instead of 3. It can be observed that, compared to the same stub implemented with 3 stages, the inductances are much smaller, and the host lines are longer, this is due to the fact that the value of the inductances is lower and therefore, the phase shift introduced by the inductances is lower, and the lines can be more similar to its original length.

Figure 4.19: Layout of the artificial transmission line of the second stub implemented with $N = 4$

The best response that has been obtained with this new parameters of the stub is shown in figure 4.20, where it can be seen that there still a disagreement with the bandwidth, this might be probably because the value of the inductances is still very high and it is not possible to achieve a more accurate response compared to the schematic.

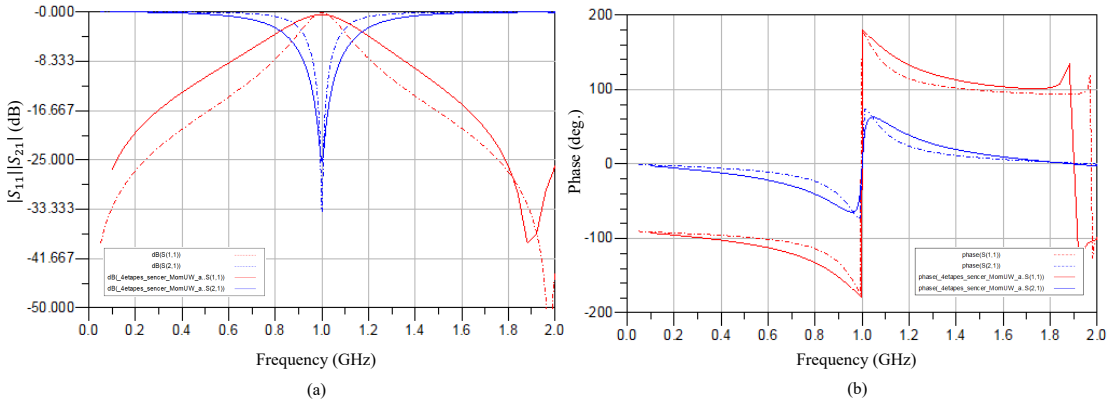

Figure 4.20: Frequency response (a) and phase (b) comparison of the second stub with $N = 4$

In order to be sure if this option is better than the one implemented with $N = 3$, in figure 4.21 is represented the response of the whole filter where the second stub is implemented with $N = 4$. It can be seen that there is still a bandwidth disagreement as this bandwidth corresponds to a 42% while the option of implementing the second stub with $N = 3$ has a bandwidth corresponding to a 40%.

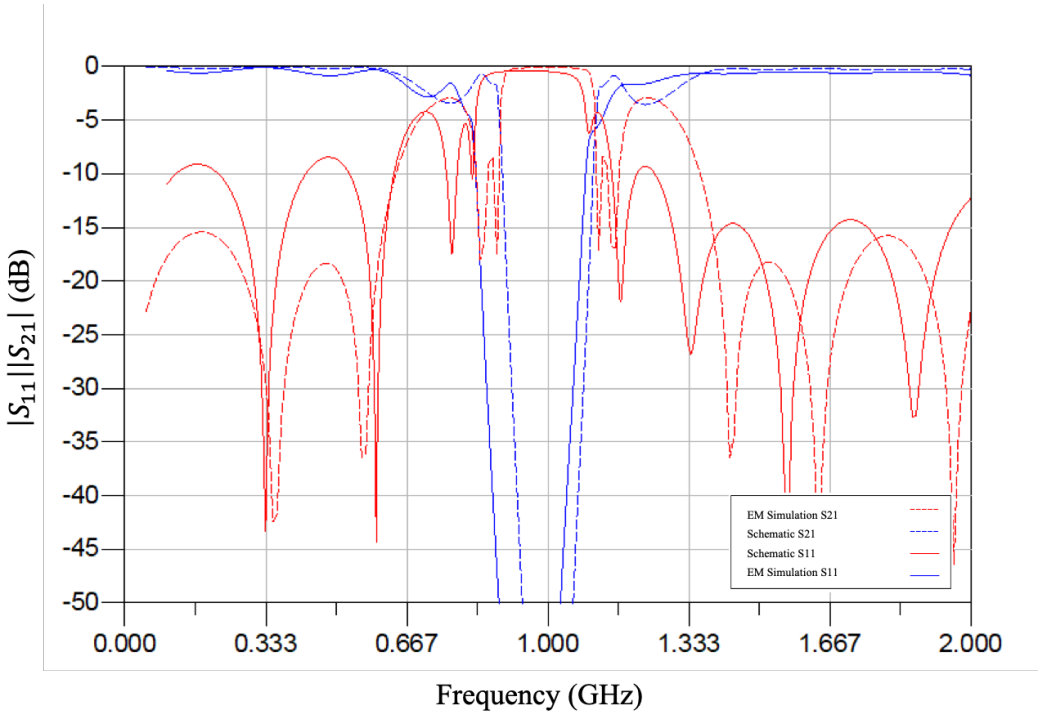

Figure 4.21: Frequency response comparison between schematic and layout of the filter implementing the second stub with N = 4

Therefore, this option is discarded as a possible solution to improve the bandwidth of the designed filter, and the filter that will be fabricated is the one where all the stubs are implemented with $N = 3$ as its response was the most suitable in terms of bandwidth.

5. PHYSICAL IMPLEMENTATION AND RESULTS COMPARISON

Once the layout design of the filter has been performed, it is the moment to implement the filter by means of a *LPFK-H100* drilling machine. An image taken from the fabricated stopband filter can be seen in figure 5.1.

Figure 5.1: Fabricated stopband filter by means of artificial transmission lines

At this point, the fabricated filter can be measured by means of the *Keysight PNA 5221A* vector network analyzer. In order to measure it, the vector network analyzer was previously calibrated.

Once the device has been tested with the vector network analyzer, the measured results can be imported to ADS in order to facilitate the comparisons between the EM simulations of the layout and the measurements, so let us represent the obtained results in figure 5.2 for the fabricated filter.

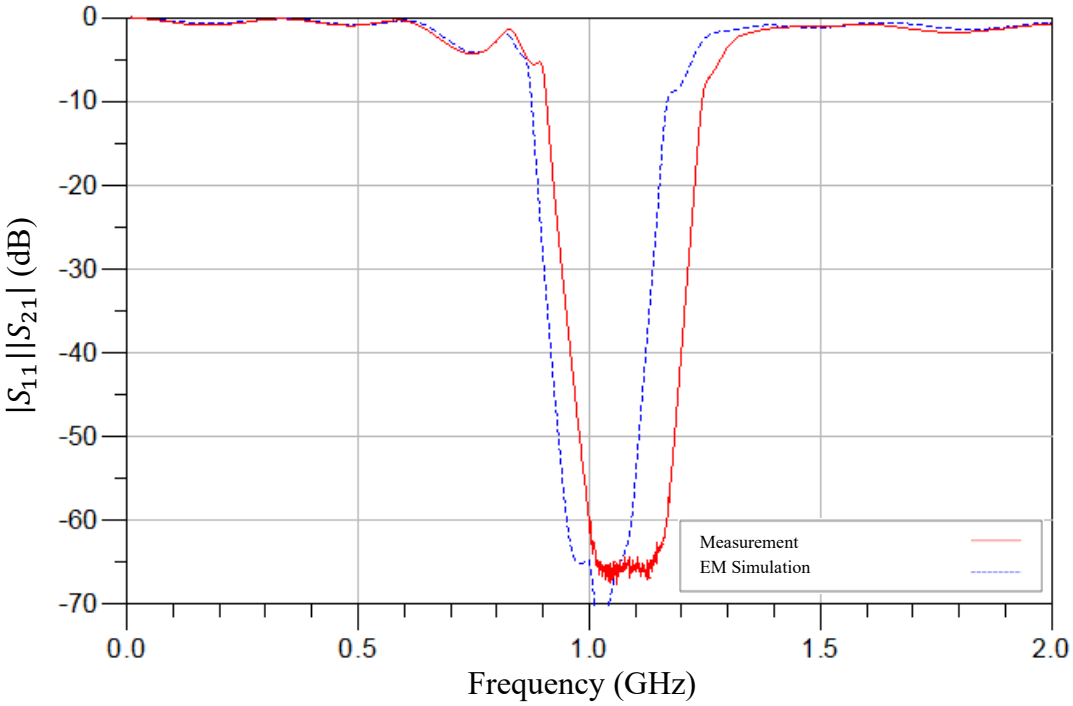

Figure 5.2: S_{21} comparison between EM simulation (dotted line) and measured filter (solid line)

As it can be seen, the response has been a bit displaced to an upper frequency and the bandwidth is a bit bigger than in the EM simulation, as it now corresponds to a 46% as it goes from $f_1 = 828MHz$ to $f_2 = 1.3GHz$, this mismatch according to the bandwidth is probably due to fabrication related tolerances.

Although, the central frequency is still very near to the desired one of 1GHz, as $f_0 = \sqrt{f_1 \cdot f_2} = 1.04GHz$.

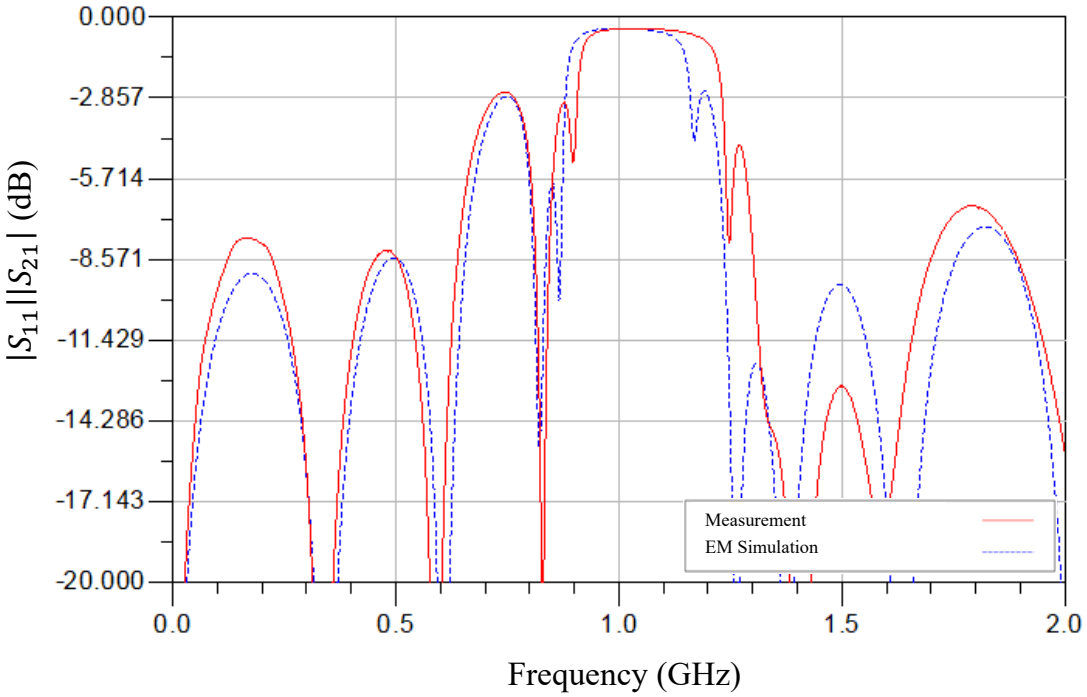

Figure 5.3: S_{11} comparison between EM simulation (dotted line) and measured filter (solid line)

For the case of the S_{11} parameter, the frequency displacement and the bandwidth increasement is also appreciated, although it can be seen that the lobes of the designed filter match quite accurately to the schematic response.

Therefore, for all the results obtained in the measurements represented in this chapter, it can be considered that the design of the stopband filter by means of artificial transmission lines, has been carried out in a quite appropriate manner.

6. CONCLUSIONS AND FUTURE LINES

In conclusion, a stopband filter implementing artificial transmission lines to the stubs has been designed and fabricated. The objectives of this thesis were to reduce the size of the filter without any increase in the complexity or cost.

As the ordinary filter was not possible to be implemented with the defined specifications because the width of the stubs was too narrow, it wasn't possible to verify that there has been a size reduction of the filter, although, it has been demonstrated that applying artificial transmission lines to the stubs, the filter is implementable using the same substrate and specifications.

Implementing the filter with ordinary lines with a bandwidth of 30% was not possible with this substrate. Even though the bandwidth ended up being 46%, the implementation of artificial transmission lines to the stubs have been a good solution as, the ordinary filter was not possible to be implemented with a bandwidth lower than 57%, as the maximum impedance value that can be implemented in this substrate is 90Ω, which corresponds to a length of $200\mu m$.

Eventually, in reference to the complexity of the design of the new filter, it is true that the design of the stubs implemented with artificial transmission lines is not as simple as in the ordinary case of the filter, even though, the cost of the filter hasn't been changed since the implementation of the inductors do not require extra materials or other special manufacturing techniques. Moreover, due to the compactness of the stubs, it allows to save more substrate area than in the case of the ordinary filter, from a fabrication process point of view.

In order to conclude this last chapter, just mention a possible further work that would consist on implementing artificial transmission lines to the host line of the filter to reduce its size horizontally.

7. REFERENCES

[1] Martin F. Artificial Transmission Lines for RF and Microwave Applications. Wiley; 2015.

[2] Orellana M, Selga J., Vélez P., Sans M., Rodríguez A., Bonache J., Boria V., Martin F. (2017). Design of Capacitively Loaded Coupled-Line Bandpass Filters with Compact Size and Spurious Suppression. *IEEE Trans Microw Theory Techn.* 2017

[3] Aznar-Ballesta F., Selga J., Vélez P., Fernández-Prieto A., Coromina J., Bonache J., & Martín F. Slow-wave coplanar waveguides based on inductive and capacitive loading and application to compact and harmonic suppressed power splitters. *International Journal of Microwave and Wireless Technologies.* 2017

[4] Vélez P, Aznar-Ballesta F, Coromina J, Bonache J, Martín F. Compact coplanar waveguide power splitter with filtering capability based on slow-wave structures. *Microw Opt Technol Lett.* 2018

[5] Pozar D. M. Chapter 8: Microwave filters. In: Microwaves Engineering. 4th Ed. United States of America; Wiley; 2012. p. 381-88

[6] Pozar D. M. Chapter 4: Microwave Network Analysis. In: Microwaves Engineering. 4th Ed. United States of America; Wiley; 2012. p. 188-95